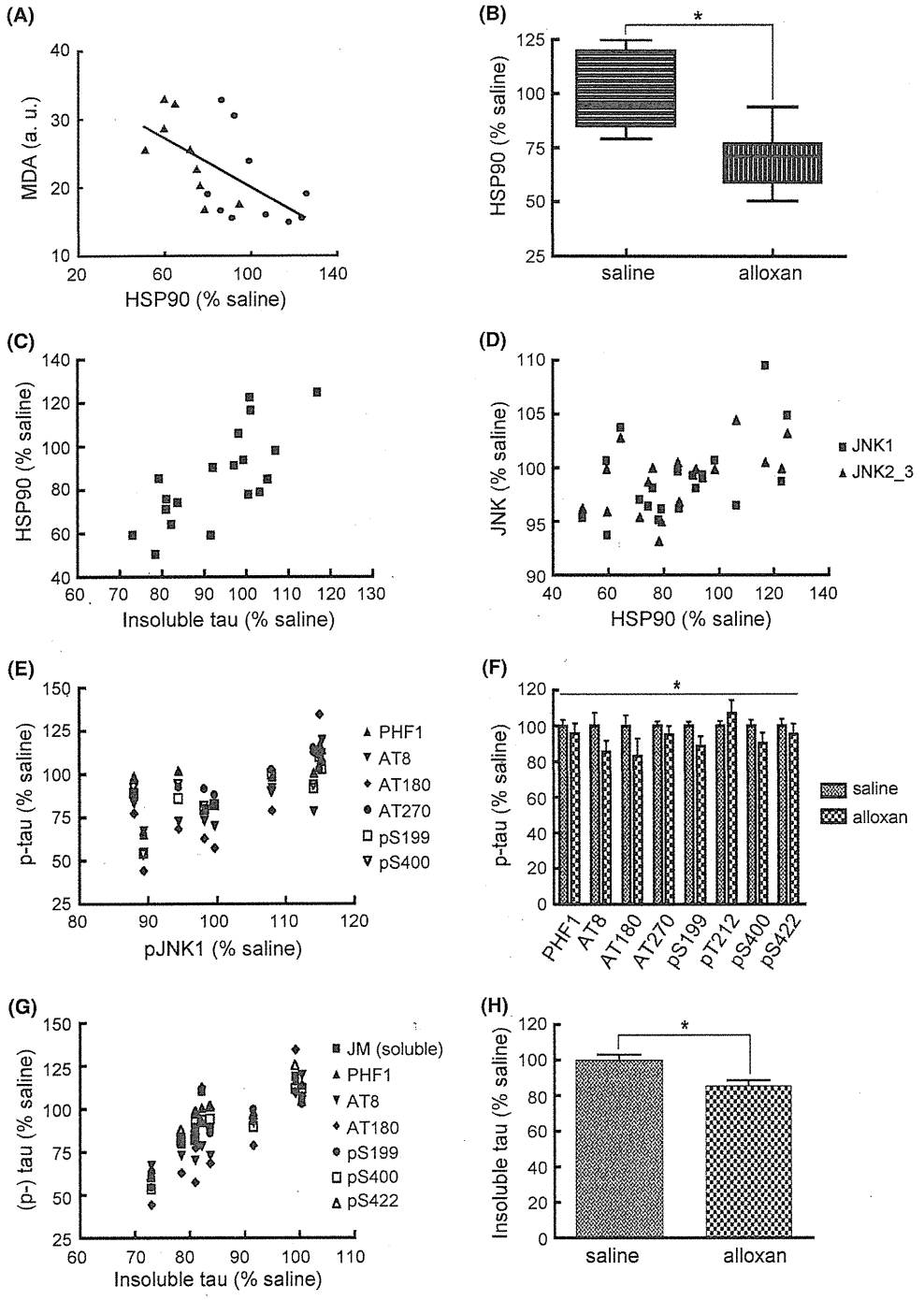

Fig. 4 Correlative changes in protein levels including reduced insoluble tau as a result of alloxan injection *in vivo*. (A) Inverse correlation between malondialdehyde and HSP90 in P301L mice ($P = 0.0074$). A trend line was drawn based on this statistical significance. Such an inverse correlation was also observed in alloxan-injected P301L mice alone as indicated by triangles ($P = 0.0201$). (B) Reduction in HSP90 levels by alloxan injections ($P = 0.0004$). (C) Positive correlation between HSP90 and insoluble tau ($P = 0.0003$). (D) Positive correlation between HSP90 and c-Jun *N*-amino terminal kinase (JNK) 1 (the lower band; $P = 0.0256$) and between HSP90 and JNK2/3 (the upper band; $P = 0.0293$). (E) Positive correlations between phospho-JNK1 and phospho-tau (PHF1, $P = 0.0463$; AT8, $P = 0.0289$; AT180, $P = 0.0056$; AT270, $P = 0.0050$; pS199, $P = 0.0190$; pS400, $P = 0.0381$) in alloxan-treated P301L mice. (F) Overall reduction in phospho-tau levels by alloxan injections ($P = 0.0064$; two-way ANOVA), even though treatment effects at individual phosphorylation sites were not statistically significant (Bonferroni post-test). (G) Significant correlations between insoluble tau and soluble tau (phospho-tau) (JM, $P = 0.0102$; PHF1, $P = 0.0022$; AT8, $P < 0.0001$; AT180, $P = 0.0120$; pS199, $P = 0.0012$; pS400, $P = 0.0023$; pS422, $P = 0.0063$) in alloxan-treated P301L mice. (H) Reduction in insoluble tau levels by alloxan injections ($P = 0.0076$).

perhaps switched on the degradation machinery that lowered GSK3β level, suppressing or counteracting the diabetogenic rise in phospho and insoluble tau levels.

We also injected alloxan into TG mice that express human mutant (R406W) tau (Tatebayashi *et al.*, 2002). These mice received three injections at half the dose (50 mg kg^{-1}) received by the former low-dose

alloxan P301L cohort (100 mg kg^{-1}). We did not detect significant changes in either blood glucose or body weight (Fig. 5A,B). We did observe, however, definite reductions in soluble pan-tau immunoreactivity but not in phospho-tau immunoreactivity in the cerebral cortices of alloxan-treated R406W mice, regardless of gender (Fig. 5C,D). The decrease in soluble tau levels significantly correlated with the decrease in insoluble tau levels (Fig. 5E,F). These changes in tau were not observed in other regions of the brain, namely hippocampus, thalamus, olfactory bulb, and striatum (Fig. S5). On the basis of these results, we suggest that alloxan has a consistent mode of action in which tau insolubilization is suppressed in the cerebral cortex of mutant tau TG mouse.

Low-dose alloxan–induced tubulin modifications indicative of microtubular stabilization

Candidate proteins that can become the clients of HSP90 and thus be the target of degradation after HSP90 inactivation are not limited to tau and JNK. HDAC6 is one such protein (Rao *et al.*, 2008). Indeed, HDAC6 was decreased in tau-expressing cells treated with either an HSP90 inhibitor, GA, or alloxan plus GSH (Fig. 1B,C). The alloxan-induced reduction in HDAC6 was prevented partially by a proteasomal inhibitor, suggesting that HDAC6 was degraded by proteasomes in response to the decrease in HSP90 (Fig. 1C). To examine the pharmacological actions of alloxan *in vivo*, we analyzed P301L mouse brain homogenates by Western blotting for HDAC6 (kFig. 6A). HDAC6 levels were decreased (Fig. 6B,C), just as HSP90 levels were decreased (Figs 3 and 4B). One of the substrates for HDAC6 is α-tubulin (Hubbert *et al.*, 2002). In GA- and alloxan-treated cell lysates, we observed increased immunoreactivity against acetylated α-tubulin (Fig. 1B,C). Proteasomal inhibition partially blocked the reduction in HDAC6 levels, which resulted in the partial reduction in acetylated tubulin levels (Fig. 1C). To test the relationship between HDAC6 and α-tubulin *in vivo*, dot blots of P301L cortical homogenates were reacted with anti-acetylated tubulin antibody (Fig. 6D). We observed an inverse correlation between HDAC6 and acetylated tubulin levels in alloxan-treated P301L mice (Fig. 6E), suggesting that the reduction in HDAC6 levels promoted tubulin acetylation (Fig. 6F). Because acetylated tubulin is present in stable microtubules (Piperno *et al.*, 1987; Hubbert *et al.*, 2002), the reduction in HDAC6 levels that resulted from the oxidative stress-related decrease in HSP90 levels might have contributed to the stabilization of microtubules through the enhancement of tubulin acetylation.

Because the detyrosinated form of α-tubulin is also present in stable microtubules (Khawaja *et al.*, 1988), next we immunostained dot blots of the same samples with anti-detyrosinated tubulin antibody (Fig. S6B). We found that alloxan treatment significantly increased detyrosinated tubulin immunoreactivity (Fig. S6D). In the P301L cohort, the parallel increase in acetylated and detyrosinated tubulin was proportional to the reduction in insoluble tau (Fig. S6A,C,E). In the R406W cohort, we also observed that alloxan treatment caused similar increases in acetylated and detyrosinated tubulin levels, which was inversely correlated with insoluble tau levels (Fig. S7). These results suggest that alloxan exerts another anti-tauopathic action: tubulin modifications that might contribute to microtubule stability.

Possible memory-enhancing effects of alloxan via reduction in HDAC2 and phospho-tau

HDAC2 is another HDAC that belongs to a class different from that of HDAC6 (Haberland *et al.*, 2009). We were interested in HDAC2 because of its relevance to memory (Guan *et al.*, 2009), because memory impairment is another phenotype associated with tauopathy. HDAC2-knockout mice display memory enhancement, while HDAC2-overexpressing mice display memory deficits (Guan *et al.*, 2009). As with HDAC6, HDAC2 levels in brain homogenates from alloxan-injected P301L mice were significantly reduced compared with those in saline-injected mice (Fig. 6G,I). The reduction in HDAC2 was also positively correlated with the reduction in HSP90 (Fig. 6H), as was HDAC6 (Fig. 6B). To determine whether this molecular event affected memory, we tested mice on the Morris water maze (MWM) test, which was conducted after alloxan injection and before sacrifice. In alloxan-injected P301L mice (Fig. S3C), stay time in the target quadrant during the probe trial (i.e., spatial memory) varied in an age-dependent manner. In alloxan-injected P301L mice, we observed a significant inverse correlation between HDAC2 levels and spatial memory (Fig. 6J). In other words, memory was enhanced as HDAC2 levels decreased, which is consistent with the findings of a previous report (Guan *et al.*, 2009).

Among the biochemical parameters that were analyzed during this study, the levels of phospho-tau, specifically AT8 and AT180, and phospho-JNK1 were also inversely proportional to spatial memory (Fig. 6K). Because some of the phospho-tau levels were also inversely correlated with MDA levels (Fig. S3D), it is possible that oxidative stress generated by alloxan perhaps in combination with aging enhanced memory by reducing the levels of phospho-tau proteins. These results suggest that mild oxidative stress may have another potentially beneficial impact on another tauopathy phenotype, namely memory deficits.

Discussion

Molecular changes induced by oxidative stress are known to accumulate with aging (Kenyon, 2010). Because the structural integrity of a molecule directs its functional capability and efficiency, events like oxidative stress that can compromise the structural integrity of a molecule are considered to be the cause of aging as well as age-related disorders (Harman, 1956; Balaban *et al.*, 2005; Kenyon, 2010). Many age-related disorders are indeed characterized by the accumulation of misfolded and aggregated proteins (Aguzzi & O'Connor, 2010). The pathological hallmark of tauopathies such as AD is neuronal inclusions of tau protein. If all forms of oxidative stress induce the accumulation of tau and tau dysfunction, then the beneficial effects of exercise on AD cannot simply be explained by the causal role of oxidative stress, considering the fact that substantial amounts of ROS are generated during exercise (Rattan & Demirović, 2010). Even though H_2O_2 accumulates with aging, it may not be the cause of aging (Cocheme *et al.*, 2011). Some reports have shown that low levels of oxidative stress can extend lifespan (Schulz *et al.*, 2007; Gems & Partridge, 2008; Heidler *et al.*, 2010; Mesquita *et al.*, 2010), indicating that certain conditions present during oxidative stress could delay aging processes. Thus, we hypothesize that a form of oxidative stress exists that counteracts pathological phenotypes associated with tau misfolding and dysfunction.

Indeed, several *in vitro* studies have demonstrated previously that ROS-generating compounds such as H_2O_2 suppress tau phosphorylation (Davis *et al.*, 1997; LoPresti & Konat, 2001; Zambrano *et al.*, 2004). In the present study, alloxan in the presence of GSH was found to act similarly as H_2O_2 in terms of tau phosphorylation but differently in terms of JNK phosphorylation, for reasons yet to be determined (Fig. S1). Because substrates of HSP90 are known to degrade when HSP90 is inactivated (Dickey *et al.*, 2007; Luo *et al.*, 2007; Nieto-Miguel *et al.*, 2008; Novoselova *et al.*, 2008), we assumed that the partial blockade of alloxan-induced reductions in tau, JNK, and HDAC6, but not HSP90, by a proteasomal inhibitor suggests that these known HSP90 substrates are degraded in

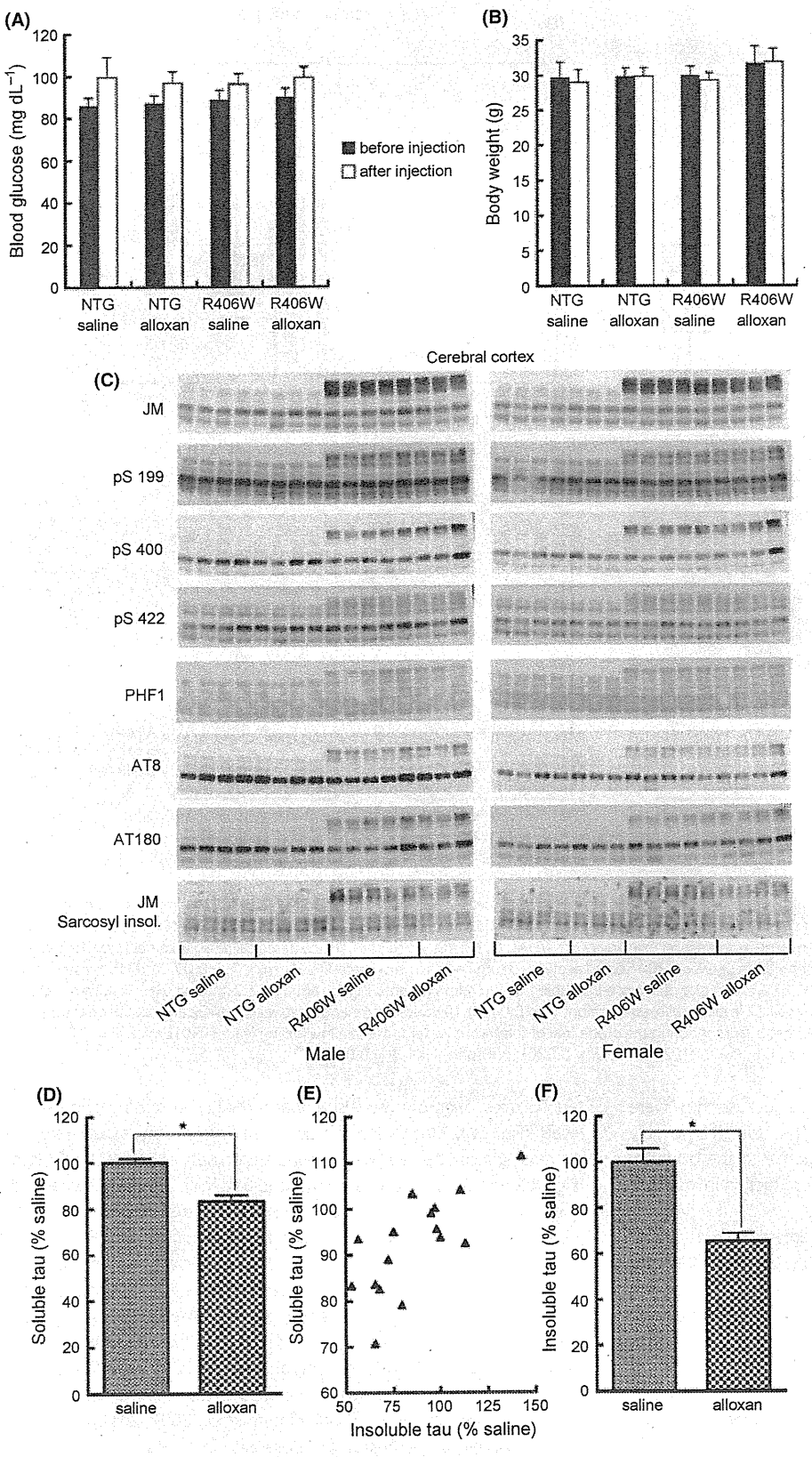

Fig. 5 Analyses of alloxan injection into R406W tau transgenic mice. No significant changes in blood glucose concentration (P = 0.7802 among groups, Friedman test; P = 0.8050 by treatment) (A) and body weight (P = 0.0839 among groups, Friedman test; P = 0.2875 by treatment) (B) in either nontransgenic or R406W mice by alloxan injections. (C) Western blot analyses of Tris-buffered saline-soluble and sarcosyl-insoluble fractions derived from the R406W cohort. (D) Quantitation of soluble tau with pan-tau antibody, JM, showing that alloxan treatment significantly reduced overall tau levels (P = 0.0002). (E) Positive correlation between soluble and insoluble tau levels in R406W mice (P = 0.0017). (F) Significant reduction in sarcosyl-insoluble tau levels in R406W mice by alloxan treatment (P = 0.0002).

response to alloxan-generated ROS (Figs 1 and S2). This is consistent with a previous report showing that ROS stimulated protein degradation in an ubiquitin-dependent manner (Medicherla & Goldberg, 2008). Although the reduction in HSP90 was consistently observed *in vitro* and *in vivo*, upregulation of other HSPs observed in the early phase of alloxan treatment *in vitro* was not detected *in vivo*. This does not necessarily mean

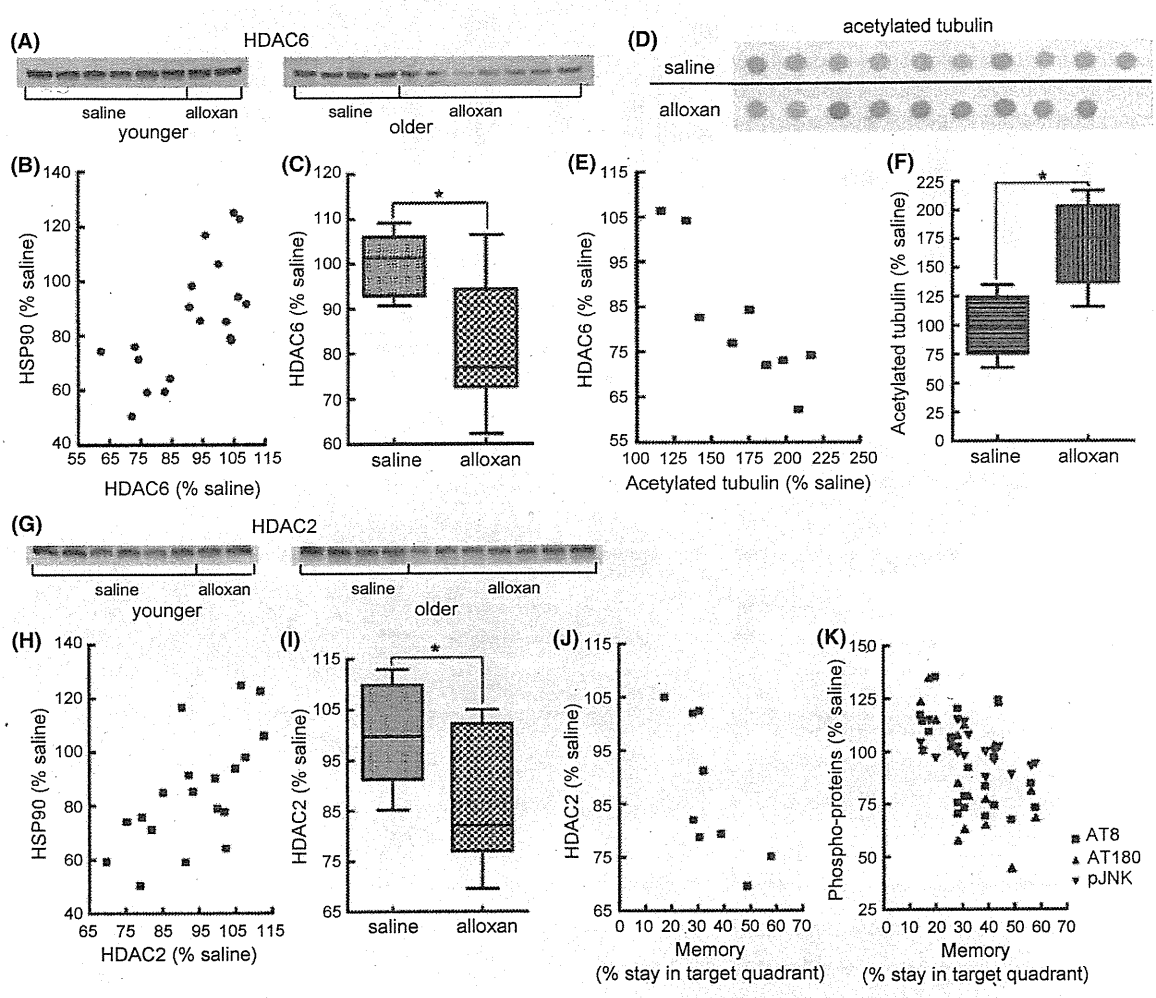

Fig. 6 Alloxan injection is associated with indications of microtubule stabilization and memory enhancement along with reductions in histone deacetylases (HDACs) and phospho-tau. (A) Western blot of sucrose-insoluble fraction derived from the brains of P301L mice. The blot was probed with anti-HDAC6 antibody. (B) Positive correlation between HSP90 and HDAC6 ($P = 0.0019$). (C) Reduction in HDAC6 levels by alloxan injections ($P = 0.0133$). (D) Dot blot of Tris-buffered saline-soluble fraction. The blot was probed with anti-acetylated tubulin antibody. (E) Inverse correlation between HDAC6 and acetylated tubulin in alloxan-treated P301L mice ($P = 0.0018$). (F) Increased acetylated tubulin levels by alloxan injections ($P = 0.0004$). (G) Western blot of sucrose-insoluble fraction. Blot was probed with anti-HDAC2 antibody. (H) Positive correlation between HSP90 and HDAC2 ($P = 0.0027$). (I) Reduction in HDAC2 levels by alloxan injections ($P = 0.0435$). (J) Inverse correlation between HDAC2 and spatial reference memory as measured by the percent (%) stay time in the target quadrant during the probe trial of the Morris water maze test in alloxan-treated P301L mice ($P = 0.0186$). (K) Inverse correlations between memory and phospho-proteins (AT8, $P = 0.0192$; AT180, $P = 0.0261$; phospho-JNK1, $P = 0.0145$).

that HSPs were not elevated in alloxan-treated mice because mice were sacrificed several weeks after the alloxan injection. Therefore, it is possible that HSP chaperones, upregulated quickly in response to the oxidative stress, suppressed tau aggregation, resulting in the reduction in insoluble tau in two mutant tau (P301L and R406W) TG mice.

In contrast to saline-injected controls, in alloxan-injected P301L mice a slight increase in MDA levels correlated with a decrease in HSP90 levels that was associated with decreased HDAC6 levels, which in turn was correlated with an increase in acetylated tubulin (Figs 3, 4 and 6). Increases in acetylated and detyrosinated tubulin levels in the two tauopathy models indicate that alloxan might contribute to microtubule stabilization by promoting both the acetylation and detyrosination of α-tubulin, producing the forms of α-tubulin contained within stabilized microtubules (Piperno *et al.*, 1987; Khawaja *et al.*, 1988) (Figs 6, S6 and S7). Furthermore, in alloxan-injected P301L mice, the reduction in HDAC2 levels was inversely proportional to enhanced memory (Fig. 6I,J), which is consistent with a previous finding (Guan *et al.*, 2009). In the future, it may be interesting to test the effects of alloxan in a paradigm of HDAC2 TG mice crossed with tau TG mice. Memory was also enhanced with decreasing phospho-tau levels (Fig. 6K). Decreasing phospho-tau levels were associated with decreasing insoluble tau levels and increasing detyrosinated tubulin levels (Figs 4G and S6E). In alloxan-treated P301L mice, because some phospho-tau levels were decreased as oxidative stress levels (i.e., MDA) increased (Fig. S3D), beneficial roles of alloxan-induced mild oxidative stress on the three phenotypes of tauopathy might be mediated via decreases in phospho-tau protein levels. This is a reasonable premise because tau phosphorylation is thought to cause tau to detach from microtubules, which then become destabilized (Mi & Johnson, 2006; Ballatore *et al.*, 2007). In turn, hyperphosphorylated tau eventually forms insoluble tau aggregates, which, perhaps in a prefibrillar state, induce synapse loss and memory deficits (Kimura *et al.*, 2007, 2010). Therefore, anti-tauopathic properties of low-dose alloxan found in mouse models can be considered as an *in vivo* proof of concept that might be assumed from *in vitro* data, such as the dephosphorylation of tau as a result of acute oxidative stress (Davis *et al.*, 1997; LoPresti & Konat, 2001; Zambrano *et al.*, 2004).

In the present study, we identified one condition associated with mild oxidative stress that ameliorates several phenotypes of tauopathy, namely the formation of tau inclusions, microtubule destabilization, and perhaps memory decline. However, other pathological outputs such as neurodegeneration were not examined in this study. Considering the toxic nature of ROS, we would expect that some neurons were also damaged in the brain as a result of the alloxan injection. Meanwhile, our previous report suggested that the substantial neuronal losses observed in P301L TG mice are the consequence of insoluble tau accumulation (Kimura *et al.*, 2010). Therefore, it is difficult to extrapolate how the alloxan-induced decrease in insoluble tau levels might influence neuronal numbers. At least *in vitro*, α-tubulin level was decreased in samples treated with overnight with alloxan (Fig. 1C). From observations of Fig. S2 (Supporting information), we suggested that this is a consequence of toxicity induced by H_2O_2 generated from alloxan. It is predicted that such a toxic impact of H_2O_2 could have affected the concentrations of variety of molecules, even those generally used as positive controls. We used β-actin and NSE as controls but detected no marked changes in their levels. The degree of toxicity to the brain and other organs resulting from the alloxan injections certainly requires further investigation. Nonetheless, in the end, we would like to emphasize once again that certain beneficial conditions associated with oxidative stress have been reported (Schulz *et al.*, 2007; Gems & Partridge, 2008; Heidler *et al.*, 2010; Mesquita *et al.*, 2010) and do exist, as demonstrated in the present study: one that induced several events that counteracted tauopathy-related phenotypes *in vivo*.

Experimental procedures

Reagents

Chemicals used in this study were purchased from the following companies: alloxan from Tokyo Kasei Kogyo (Tokyo, Japan); GSH, H_2O_2, SDS and sarcosyl from Nacalai, Kyoto, Japan; lactacystin from Milliore (Billerica, MA, USA); geldanamycin, dimethyl sulfoxide, catalase, and deferoxamine from Sigma-Aldrich (St. Louis, MO, USA).

Cell culture

For analyzing the acute effects of alloxan treatment on neuronal cells *in vitro*, we used the Neuro2A cell line, which stably expresses Myc-tagged tau (P301L); it was previously established by infecting neuroblastoma cells with retrovirus harboring cDNA-encoding Myc-tagged tau (P301L) and through puromycin selection (Hatakeyama *et al.*, 2004). The cells were cultured under an atmosphere of 5% CO_2 at 37 °C in Dulbecco's modified Eagle's medium (Sigma-Aldrich) supplemented with 10% fetal calf serum (Thermo Scientific, South Logan, UT, USA), gentamycin (Invitrogen, Camarillo, CA, USA), puromycin (Nacalai), and G418 (Nacalai). Two days before treatment, cells were plated onto six-well plates (Corning, Corning, NY, USA) at 5.5–6.0 × 10^5 cells per well in medium without puromycin and G418. After being rinsed with PBS, cells were lysed by homogenization in Tris-buffered saline [TBS; 10 mM Tris, 150 mM NaCl (pH 7.4), 1 mM EDTA, 1 mM EGTA] or by sonication either in modified RIPA buffer [50 mM Tris (pH 7.4), 1%·NP-40, 0.25% sodium deoxycholate, 150 mM NaCl, 1 mM EGTA] or in 2% SDS, depending on each experiment as specified in the figure legends. All lysis solutions contained protease inhibitors (5 μg mL^{-1} pepstatin, 5 μg mL^{-1} leupeptin, 2 μg mL^{-1} aprotinin, and 0.5 mM 4-(2-aminoethyl)benzenesulfonyl fluoride hydrochloride) and phosphatase inhibitors (1 μM okadaic acid, 1 mM Na_3VO_4, and 1 mM NaF). After centrifugation at 100 000 *g* for 30 min (or 20 000 *g* for 20 min when TBS lysis buffer was used) at 4 °C, the supernatant was collected and its total protein concentration was measured and normalized with the Bradford method.

Immunoblotting

Some samples were solubilized in Laemmli sample buffer and subjected to SDS–PAGE and then to Western blotting. Other samples were directly blotted onto a nitrocellulose membrane for dot blot analysis. Membranes were incubated with primary antibody followed by a species-appropriate HRP-conjugated secondary antibody. Chemiluminescent detection (GE Healthcare, Piscataway, NJ, USA) was used for visualization. The primary antibodies used were antibodies against total tau (anti-pan-tau or tau5, Biosource; or JM, developed in our laboratory); phosphorylated tau (PHF1, generously provided by Dr. Peter Davies, Albert Einstein College of Medicine, NY); AT8, AT180, and AT270 (Innogenetics, Gent, Belgium); pS199, pT212, pT231, pS400, and pS422 (Invitrogen); pS262 (Anaspec, Fremont, CA, USA); tau1 (Millipore, Billerica, MA, USA), which recognizes dephosphorylated tau at Ser-199 and Ser-202; JNK, phospho-JNK, AKT1, phospho-GSK3β, p38 MAPK, and phsopho-p38 MAPK (Cell Signaling, Danvers, MA, USA); GSK3β (BD Transduction, Franklin Lakes, NJ, USA); MARK2 (Abgent, San Diego, CA, USA); phopho-MARK2 (IBL, Gunma, Japan); PP2A-c (Millipore); demethyl PP2A-c, CaM kinase II, phospho-CaM kinase II, and HDAC6 (Santa Cruz Biotechnology, Santa Cruz, CA, USA); HSP90, HSP70, and HSP40 (Enzo Life Sciences, Farmingdale, NY, USA); HSP27 and detyrosinated tubulin (Millipore); α-tubulin and acetylated tubulin (Sigma-Aldrich); ubiquitin (Enzo Life Sciences); and HDAC2 (Abcam, San Francisco, CA, USA). Quantification and visual analysis of immunoreactivity were performed with a computer-linked LAS-3000 Bio-Imaging Analyzer System (Fujifilm, Tokyo, Japan). Statistical analyses were conducted using PRISM4 (GraphPad Software, La Jolla, CA, USA). The significance of treatment effects was confirmed by two-tailed Mann–Whitney test unless otherwise stated in each figure legend. For the analyses of 'high-dose' P301L cohort, unpaired *t*-test was used because paired *t*-test requires three or more pairs (Fig. S4D). Friedman test was used to detect differences between groups. Significance of linear dependency was tested with Pearson's correlation. All data in this study are presented as means ± SEM.

Animals

We used hemizygous tau mice on a C57BL/6J background. The mice were derived from two lines that express human tau containing a mutation (P301L or R406W) associated with frontotemporal dementia with parkinsonism linked with chromosome 17 (FTDP-17) (Tatebayashi *et al.*, 2002; Kimura *et al.*, 2010). Expression of mutant human tau was driven by CaM kinase II promoter, as described previously (Tatebayashi *et al.*, 2002; Kimura *et al.*, 2010). The P301L cohort (P301L TG and NTG controls) consisted of only males, while the R406W cohort (R406W TG and NTG controls) consisted of both males and females at approximately a 1:1 ratio. The 'low-dose' P301L cohort (20- to 27-month-old) was given an intraperitoneal injection of either alloxan (100 mg kg^{-1} in a volume of 8.0 mL kg^{-1}) or saline vehicle in their home cages. Thus, the 'low-dose' P301L cohort was divided into four groups, each containing the following number of animals: 11 NTG mice treated with saline, 11 NTG mice treated with alloxan, 10 P301L TG mice treated with saline, and nine P301L TG mice treated with alloxan. After conducting behavioral tests, including the Morris water maze or MWM as described previously (Kimura *et al.*, 2007), mice were sacrificed. The 'high (diabetogenic)-dose' P301L cohort (11- to 14-month-old) was given an intraperitoneal injection of either

alloxan (300 mg kg^{-1} in a volume of 12.0 mL kg^{-1}) or saline vehicle. Within 10 days after the injection, 73.3% of 300 mg kg^{-1} alloxan-injected mice had died. Thus, the final number of animals in 'high-dose' P301L cohort was four NTG mice treated with saline, two NTG mice treated with alloxan, four P301L TG mice treated with saline, and two P301L TG mice treated with alloxan. Behavioral tests were not performed for this cohort.

In the meantime, the R406W cohort (22- to 25-month-old) was given three intraperitoneal injections, at an interval of 2 weeks between injections, of either alloxan (50 mg kg^{-1} in a volume of 8.0 mL kg^{-1}) or saline vehicle in their home cages. The breakdown for the R406W cohort was eight NTG mice treated with saline, seven NTG mice treated with alloxan, ten R406W TG mice treated with saline, and seven R406W TG mice treated with alloxan. Approximately 1 month after the injections, the cohort of R406W mice was sacrificed. The MWM test was not conducted beforehand.

At two points during the course of experiments, just before injection and before sacrifice, blood glucose levels and body weight were measured after overnight fasting. Blood was taken from the tale, and glucose content was measured with an Accu-Chek Aviva blood glucose monitor (Roche, Basel, Switzerland).

Mouse brains were homogenized in TBS containing protease inhibitors and phosphatase inhibitors, as described in the Cell culture section. After centrifugation at 20 000 *g* for 15 min at 4 °C, the supernatant was collected as the (TBS) 'soluble' fraction. Sarcosyl-insoluble, paired helical filament-enriched fractions were prepared from the TBS-insoluble pellets according to the procedure developed by Greenberg and Davies (Greenberg & Davis, 1990). The resulting precipitate was re-homogenized in five volumes of 0.8 M NaCl and 10% sucrose solution and centrifuged at 20 000 *g* for 15 min at 4 °C. Then, 1% SDS at a volume four times the brain weight was added to the pellet, which was sonicated to make the 'sucrose-insoluble' fraction. MDA levels in this fraction were measured using an assay kit (Bioxytech MDA-586; OXIS International, Beverly Hills, CA, USA) for reducing nonspecific reactions with Tris according to the manufacturer's protocol. Meanwhile, a one-tenth volume of 10% sarcosyl solution was added to the sucrose-soluble supernatant, which was then mixed by vortex, incubated for 1 h at 37 °C, and centrifuged at 150 000 *g* for 1 h at 4 °C. The resulting pellet was solubilized in Laemmli sample buffer and analyzed as the (sarcosyl) 'insoluble' fraction. All experiments using mice were performed according to procedures approved by the Animal Care and Use Committee of the Institute of Physical and Chemical Research (RIKEN, Saitama, Japan).

Acknowledgments

This work was supported by a grant-in-aid for Scientific Research on Priority Areas (Research on Pathomechanisms on Brain Disorders) from the Ministry of Education, Culture, Sports, Science, and Technology of Japan. Authors have no competing financial interests to declare.

Author contributions

Y.Y. and A.T. designed the experiments and wrote the manuscript. Y.Y., S.Y., T.M., and T.K. performed mouse behavioral analyses. Y.Y., S.M., and Y.S. performed the *in vitro* experiments. Y.Y., M.M., and N.S. worked on the biochemical analysis of mouse brain homogenates.

References

Aguzzi A, O'Connor T (2010) Protein aggregation diseases: pathogenicity and therapeutic perspectives. *Nat. Rev. Drug Discov.* **9**, 237–248.

Balaban RS, Nemoto S, Finkel T (2005) Mitochondria, oxidants, and aging. *Cell* **120**, 483–495.

Ballatore C, Lee VM-Y, Trojanowski JQ (2007) Tau-mediated neurodegeneration in Alzheimer's disease and related disorders. *Nat. Rev. Neurosci.* **8**, 663–672.

Braak H, Braak E (1996) Evolution of the neuropathology of Alzheimer's disease. *Acta Neurol. Scand. Suppl.* **165**, 3–12.

Clodfelder-Miller BJ, Zmijewska AA, Johnson GVW, Jope RS (2006) Tau is hyperphosphorylated at multiple sites in mouse brain *in vivo* after streptozotocin-induced insulin deficiency. *Diabetes* **55**, 3320–3325.

Cocheme HM, Quin C, McQuaker SJ, Cabreiro F, Logan A, Prime TA, Abakumova I, Patel JV, Fearnley IM, James AM, Porteous CM, Smith RAJ, Saeed S, Carre JE, Singer M, Gems D, Hartley RC, Partridge L, Murphy MP (2011) Measurement of H_2O_2 with living Drosophila during aging using a ratiometric mass spectrometry probe targeted to the mitochondrial matrix. *Cell Metab.* **13**, 340–350.

Davis DR, Anderton BH, Brion J-P, Reynolds CH, Hanger DP (1997) Oxidative stress induces dephosphorylation of τ in rat brain primary neuronal cultures. *J. Neurochem.* **68**, 1590–1597.

Dias-Santagata D, Fulga TA, Duttaroy A, Feany MB (2007) Oxidative stress mediates tau-induced neurodegeneration in Drosophila. *J. Clin. Invest.* **117**, 236–245.

Dickey CA, Kamal A, Lundgren K, Klosak N, Bailey RM, Dunmore J, Ash P, Shoraka S, Zlatkovic J, Eckman CB, Patterson C, Dickson DW, Nahman Jr NS, Hutton M, Burrows F, Petrucelli L (2007) The high-affinity HSP90-CHIP complex recognizes and selectively degrades phosphorylated tau client proteins. *J. Clin. Invest.* **117**, 648–658.

Gems D, Partridge L (2008) Stress-response hormesis and aging: ''That which does not kill us makes us stronger''. *Cell Metab.* **7**, 200–203.

Genet S, Kale RK, Baquer NZ (2002) Alterations in antioxidant enzymes and oxidative damage in experimental diabetic rat tissues: effect of vanadate and fenugreek (*Trigonella foenum graecum*). *Mol. Cell. Biochem.* **236**, 7–12.

Greenberg SG, Davis P (1990) A preparation of Alzheimer paired helical filaments that displays distinct τ proteins by polyacrylamide gel electrophoresis. *Proc. Natl Acad. Sci. USA* **87**, 5827–5831.

Guan J-S, Haggarty SJ, Giacometti E, Dannenberg J-H, Joseph N, Gao J, Nieland TJF, Zhou Y, Wang X, Mazitschek R, Bradner JE, DePinho RA, Jaenisch R, Tsai L-H (2009) HDAC2 negatively regulates memory formation and synaptic plasticity. *Nature* **459**, 55–63.

Haberland M, Montgomery RL, Olson EN (2009) The many roles of histone deacetylases in development and physiology: implications for disease and therapy. *Nat. Rev. Genet.* **10**, 32–42.

Harman D (1956) Aging: a theory based on free radical and radiation chemistry. *J. Gerontol.* **11**, 298–300.

Hatakeyama S, Matsumoto M, Kamura T, Murayama M, Chui DH, Planel E, Takahashi R, Nakayama KI, Takashima A (2004) U-box protein carboxyl terminus of Hsc70-interacting protein (CHIP) mediates poly-ubiquitylation preferentially on four-repeat Tau and is involved in neurodegeneration of tauopathy. *J. Neurochem.* **91**, 299–307.

Heidler T, Hartwig K, Daniel H, Wenzel U (2010) *Caenorhabditis elegans* lifespan extension caused by treatment with an orally active ROS-generator is dependent on DAF-16 and SIR-2.1. *Biogerontology* **11**, 183–195.

Hubbert C, Guardiola A, Shao R, Kawaguchi Y, Ito A, Nixon A, Yoshida M, Wang X-F, Yao TP (2002) HDAC6 is a microtubule-associated deacetylase. *Nature* **417**, 455–458.

Hutton M (2000) Molecular genetics of chromosome 17 tauopathies. *Ann. N Y Acad. Sci.* **920**, 63–73.

Kenyon CJ (2010) The genetics of ageing. *Nature* **464**, 504–512.

Khawaja S, Gundersen GG, Bulinski JC (1988) Enhanced stability of microtubules enriched in detyrosinated tubulin is not a direct function of detyrosination level. *J. Cell Biol.* **106**, 141–149.

Kimura T, Yamashita S, Fukuda T, Park J-M, Murayama M, Mizoroki T, Yoshiike Y, Sahara N, Takashima A (2007) Hyperphosphorylated tau in parahippocampal cortex impairs place learning in aged mice expressing wild-type human tau. *EMBO J.* **26**, 5143–5152.

Kimura T, Fukuda T, Sahara N, Yamashita S, Murayama M, Mizoroki T, Yoshiike Y, Lee B, Sotiropoulos I, Maeda S, Takashima A (2010) Aggregation of detergent-insoluble tau is involved in neuronal loss but not in synaptic loss. *J. Biol. Chem.* **285**, 38692–38699.

Kulic L, Wollmer MA, Rhein V, Paganj L, Kuehnle K, Cattepoel S, Tracy J, Eckert A, Nitsch RM (2009) Combined expression of tau and the Harlequin mouse

mutation leads to increased mitochondrial dysfunction, tau pathology and neurodegeneration. *Neurobiol. Aging* **32**, 1827–1838.
Lenzen S (2008) The mechanism of alloxan- and streptozotocin-induced diabetes. *Diabetologia* **51**, 216–226.
Lenzen S, Panten U (1988) Alloxan: history and mechanism of action. *Diabetologia* **31**, 337–342.
LoPresti P, Konat GW (2001) Hydrogen peroxide induces transient dephosphorylation of tau protein in cultured rat oligodendrocytes. *Neurosci. Lett.* **311**, 142–144.
Luo W, Dou F, Rodina A, Ship S, Kim J, Zhao Q, Moulick K, Aguirre J, Wu N, Greengard P, Chiosis G (2007) Roles of heat-shock protein 90 in maintaining and facilitating the neurodegenerative phenotype in tauopathies. *Proc. Natl Acad. Sci. USA* **104**, 9511–9516.
Mattson MP (2008) Awareness of hormesis will enhance future research in basic and applied neuroscience. *Crit. Rev. Toxicol.* **38**, 633–639.
Medicherla B, Goldberg AL (2008) Heat shock and oxygen radicals stimulate ubiquitin-dependent degradation mainly of newly synthesized proteins. *J. Cell Biol.* **182**, 663–673.
Mesquita A, Weinberger M, Silva A, Sampaio-Marques B, Almeida B, Leao C, Costa V, Rodrigues F, Burhans WC, Ludovico P (2010) Caloric restriction or catalase inactivation extends yeast chronological lifespan by inducing H_2O_2 and superoxide dismutase activity. *Proc. Natl Acad. Sci. USA* **107**, 15123–15128.
Mi K, Johnson GV (2006) The role of tau phosphorylation in the pathogenesis of Alzheimer's disease. *Curr. Alzheimer Res.* **3**, 449–463.
Nieto-Miguel T, Gajate C, Gonzalez-Camacho F, Mollinedo F (2008) Proapoptotic role of Hsp90 by its interaction with c-Jun N-terminal kinase in lipid rafts in edelfosine-mediated antileukemic therapy. *Oncogene* **27**, 1779–1787.
Novoselova TV, Cherenkov DA, Khrenov MO, Glushkova OV, Lunin SM, Novoselova EG, Fesenko EE (2008) Effect of geldanamycin on the expression of signal proteins and heat shock proteins in normal mice lymphocytes. *Tsitologiia* **50**, 629–635.
Perez VI, Buffenstein R, Masamsetti V, Leonard S, Salmon AB, Mele J, Andziak B, Yang T, Edrey Y, Friguet B, Ward W, Richardson A, Chaudhuri A (2009) Protein stability and resistance to oxidative stress are determinants of longevity in the longest-living rodent, the naked mole-rat. *Proc. Natl Acad. Sci. USA* **106**, 3059–3064.
Piperno G, LeDizet M, Chang XJ (1987) Microtubules containing acetylated α-tubulin in mammalian cells in culture. *J. Cell Biol.* **104**, 289–302.
Rao R, Fiskus W, Yang Y, Lee P, Joshi R, Fernandez P, Mandawat A, Atadja P, Bradner JE, Bhalla K (2008) HDAC6 inhibition enhances 17-AAG—mediated abrogation of hsp90 chaperone function in human leukemia cells. *Blood* **112**, 1886–1893.
Rattan SIS, Demirovic D (2010) Hormesis can and does work in humans. *Dose-Response* **8**, 58–63.
Schulz TJ, Zarse K, Voigt A, Urban N, Birringer M, Ristow M (2007) Glucose restriction extends *Caenorhabditis elegans* life span by inducing mitochondrial respiration and increasing oxidative stress. *Cell Metab.* **6**, 280–293.
Siddiqui MR, Taha A, Moorthy K, Hussain ME, Basir SF, Baquer NZ (2005) Amelioration of altered antioxidant status and membrane linked functions by vanadium and Trigonella in alloxan diabetic rat brains. *J. Biosci.* **30**, 483–490.
Sigenaga MK, Hagen TM, Ames BN (1994) Oxidative damage and mitochondrial decay in aging. *Proc. Natl Acad. Sci. USA* **91**, 10771–10778.
Tatebayashi Y, Miyasaka T, Chui D-H, Akagi T, Mishima K, Iwasaki K, Fujisawa M, Tanemura K, Murayama M, Ishiguro K, Planel E, Sato S, Hashikawa T, Takashima A (2002) Tau filament formation and associative memory deficit in aged mice expressing mutant (R406W) human tau. *Proc. Natl Acad. Sci. USA* **99**, 13896–13901.
Van Remmen H, Ikeno Y, Hamilton M, Pahlavani M, Wolf N, Thorpe SR, Alderson NL, Baynes JW, Epstein CJ, Huang TT, Nelson J, Strong R, Richardson A (2003) Life-long reduction in MnSOD activity results in increased DNA damage and higher incidence of cancer but does not accelerate aging. *Physiol. Genomics* **16**, 29–37.
Yen SH, Liu WK, Hall FL, Yan SD, Stern D, Dickson DW (1995) Alzheimer neurofibrillary lesions: molecular nature and potential roles of different components. *Neurobiol. Aging* **16**, 381–387.
Zambrano CA, Egana JT, Nunez MT, Maccioni RB, Gonzalez-Billault C (2004) Oxidative stress promotes τ dephosphorylation in neuronal cells: the roles of Cdk5 and PP1. *Free Radic. Biol. Med.* **36**, 1393–1402.
Zhu X, Raina AK, Lee H-G, Casadesus G, Smith MA, Perry G (2004) Oxidative stress signalling in Alzheimer's disease. *Brain Res.* **1000**, 32–39.

Supporting Information

Additional supporting information may be found in the online version of this article:

Fig. S1 Time-dependent alterations in protein levels caused by alloxan and H_2O_2 treatments.

Fig. S2 H_2O_2 generated from alloxan as the responsible factor for changes in protein levels.

Fig. S3 Correlative changes induced by low-dose alloxan injection in P301L mice.

Fig. S4 High-dose alloxan–induced changes in P301L mice.

Fig. S5 Western blot analyses of four brain regions of R406W cohort.

Fig. S6 Low-dose alloxan–induced tubulin modifications in P301L mice.

Fig. S7 Low-dose alloxan–induced tubulin modifications in R406W mice.

As a service to our authors and readers, this journal provides supporting information supplied by the authors. Such materials are peer-reviewed and may be re-organized for online delivery, but are not copy-edited or typeset. Technical support issues arising from supporting information (other than missing files) should be addressed to the authors.

FULL PAPER *Pathology*

Binding of Curcumin to Senile Plaques and Cerebral Amyloid Angiopathy in the Aged Brain of Various Animals and to Neurofibrillary Tangles in Alzheimer's Brain

Mayu MUTSUGA[1)], James Kenn CHAMBERS[1)], Kazuyuki UCHIDA[1)], Meina TEI[1)], Takao MAKIBUCHI[2)], Tatsuya MIZOROGI[3)], Akihiko TAKASHIMA[3)] and Hiroyuki NAKAYAMA[1)]*

[1)]*Department of Veterinary Pathology, Graduate School of Agricultural and Life Sciences, The University of Tokyo, 1–1–1 Yayoi, Bunkyo-ku, Tokyo 113–8657, Japan*
[2)]*National Saigata Hospital, Joetsu-shi, Niigata 949–3193, Japan*
[3)]*RIKEN, Brain Science Institute, 2–1 Hirosawa, Wako-shi, Saitama 351–0198, Japan*

(Received 29 June 2011/Accepted 19 August 2011/Published online in J-STAGE 2 September 2011)

ABSTRACT. The binding of curcumin to senile plaques (SPs) and cerebral amyloid angiopathy (CAA) was examined in the aged brain of various animal species and a human patient with Alzheimer's disease (AD), together with its binding to neurofibrillary tangles (NFTs). Brain sections were immunostained with anti-amyloid β protein 1–42 (Aβ42) and anti-amyloid β protein 1–40 (Aβ40) antibodies. These sections were also stained with alkaline Congo red, periodic acid-methenamine silver (PAM), and curcumin (0.009% curcumin solution) with or without formic acid pretreatment. The sections from the AD brain were also immunostained for anti-paired helical filament-tau (PHF-tau), and were stained with Gallyas silver for NFTs. Some SPs in the AD, monkey, dog, bear, and amyloid precursor protein transgenic mouse (APP Tg-mouse) brains contained congophilic materials, and were intensely positive for curcumin. In addition, curcumin labeled some diffuse SPs negative for Congo red in the AD, monkey, bear, and APP Tg-mouse brains. In all animals, CAA was intensely positive for both Congo red and curcumin. The specific curcumin staining activity was lost by formic acid pretreatment. In the AD brain, NFTs positive for PHF-tau and Gallyas silver were moderately stained with curcumin. These findings indicate that curcumin specifically binds to the aggregated Aβ molecules in various animals, and further to phosphorylated tau protein, probably according to its conformational nature.

KEY WORDS: β amyloid, cerebral amyloid angiopathy, curcumin, neurofibrillary tangle, senile plaque.

doi: 10.1292/jvms.11-0307; *J. Vet. Med. Sci.* 74(1): 51–57, 2012

Senile plaques (SPs), cerebral amyloid angiopathy (CAA), and neurofibrillary tangles (NFTs) are the most characteristic histopathological features in the brains of patients with Alzheimer's disease (AD). SPs and CAA consist of amyloid β protein (Aβ), and they are detected by Congo red or periodic acid-methenamine silver (PAM) staining. SPs are morphologically classified into two types: diffuse plaques (DPs) and mature plaques (MPs). DPs are the earliest stage of plaque formation, and negative for Congo red [29]. MPs are the progressive stage of Aβ aggregation and positive for Congo red [28]. MPs also have swollen neurites or glial hallow. On the other hand, NFTs are formed in the cytoplasm of a neuron as aggregates of highly phosphorylated tau, a microtubule-associated protein. NFTs are detected clearly by Gallyas silver staining. These histopathological features are frequently observed in the aged brains of various nonhuman animal species. SPs and CAA have been observed in the brain of aged nonhuman primates [7, 17, 21, 24], dogs [3, 9, 16, 24, 26], cats [18], a camel [19], bears [6, 27], a wolverine [22], and a great spotted woodpecker [20], whereas NFTs have been reported only in a chimpanzee [23], sheep [5], bears [6], and a wolverine [22].

Curcumin, a yellow phenolic pigment and an ingredient for curry, has potent protective and curative activities against neoplastic-, inflammatory-, amyloid and oxidant-associated disorders [1, 8, 13]. It has been reported that curcumin binds to Aβ aggregates *in vivo* and inhibits the formation of SPs [2, 10, 11, 30]. Because of its specific binding ability, use of curcumin has been expected to prevent or treat AD. Recent investigations have demonstrated that SPs, CAA, and NFTs are detected by curcumin staining in AD model mice (APPswe/PS1dE9 mice) [10] as well as AD brains [14]. However, such binding of curcumin is not well known in animals other than mouse and human.

In the present study, we examined the binding of curcumin to SPs and CAA in the aged brain of various animal species, and to NFTs in the AD brain.

MATERIALS AND METHODS

Tissue samples and histology: We examined the cerebral cortex from an AD patient, a Japanese macaque, dogs, a cat, an American black bear, a Bactrian camel, a great spotted woodpecker, and an amyloid precursor protein transgenic mouse (APP Tg-mouse) (APP23, The Jackson Laboratory, Bar Harbor, ME, U.S.A.). Sex, age, and breed of the animals are shown in Table 1. Brain tissue samples were fixed

* CORRESPONDENCE TO: NAKAYAMA, H., Department of Veterinary Pathology, Graduate School of Agricultural and Life Sciences, The University of Tokyo, 1–1–1 Yayoi, Bunkyo-ku, Tokyo 113–8657, Japan.
e-mail: anakaya@mail.ecc.u-tokyo.ac.jp

Table 1. Histopathologic features of the brain of the aged animals examined

Case No.	Species	Breed or remark	Sex	Age	SPs		CAA	NFT
					DP	MP		
1	Human	AD patient	Female	73y	+	+	+	+
2	Japanese macaque	NA	unknown	>26y	+	+	+	–
3	Dog	Miniture.dax	Female	13y	+	–	+	–
4	Dog	Beagle	Male	14y	+	–	+	–
5	Dog	Mongrel	Male	14y	+	+	+	–
6	Dog	unknown	unknown	14y	+	+	+	–
7	Dog	unknown	unknown	18y	+	+	+	–
8	Dog	Maltese	unknown	18y	+	–	+	–
9	Dog	Mongrel	Female	20y	+	–	+	–
10	Cat	Monglel	Female	20y	+	–	+	–
11	American black bear	NA	Female	20y	+	+	+	–
12	Bactrian camel	NA	Female	>20y	+	–	–	–
13	Great spotted woodpecker	NA	Male	>16y	–	–	+	–
14	Mouse	APP23Tg	Female	30m	+	+	+	–

SP: Senile plaque, DP: Diffuse plaque, MP: Mature plaque, CAA: Cerebral amyloid angiopathy, NFT: Neurofibrillary tangle, y: Years, m: Months, and NA: Not applicable.

in a 10% neutral-buffered formalin solution and embedded in paraffin by a routine procedure.

Paraffin sections (4 to 8 μm thick) were stained with alkaline Congo red or PAM to detect SPs and CAA. In addition, sections from the AD brain were stained with Gallyas silver [4] to detect NFTs. The sections were preferably compared at the same regions.

Immunohistochemistry: Immunostaining with anti-Aβ1-42 (Aβ42: BC05, Aβ-Protein Immunohistostain Kit, Wako, Osaka, Japan) and anti-Aβ 1-40 (Aβ40: BA27, Aβ-Protein Immunohistostain Kit, Wako) antibodies was carried out in accordance with the manufacturer's procedure for the Aβ-Protein Immunohistostain Kit (Wako). Immunostaining with anti-PHF-tau antibody (PHF-tau: AT8, 10 μg/m*l*, Thermo, Kanagawa, Japan) was carried out in the following methods. Deparaffinized sections were first autoclaved at 120°C for 10 min in 10 mM citrate buffer for antigen retrieval. Tissue sections were then treated with 1% hydrogen peroxide in methanol for 3 min to inhibit endogenous peroxidase activity and further incubated in 8% skimmed milk in tris-buffered saline (TBS) at 37°C for 30 min to block nonspecific reactions. The sections were incubated with a primary antibody at 4°C overnight. Following 3 washings in TBS, sections were then incubated with an HRP-labeled polymer-conjugated secondary antibody against mouse IgG (Dako Japan, Kyoto, Japan) at 37°C for 60 min. Finally, the reaction products were visualized with 0.05% 3-3'-diaminobenzidine and 0.03% hydrogen peroxide in tris–HCl buffer. Counterstaining was carried out with Mayer's hematoxylin.

Curcumin staining: Deparaffinized sections were immersed in 80% ethanol, 0.3% Triton X-100, and 0.1 M TBS (pH 7.4) containing 3% bovine serum albumin (BSA) and 0.5% Tween 20, for 10 min each. Curcumin powder (Cayman Chemical Company, Ann Arbor, MI, U.S.A.) was resolved in 0.1 M TBS (pH 7.4) containing 3% BSA and 0.5% Tween 20 at 25 μM (0.009% curcumin solution). Sections were incubated with the curcumin solution at 37°C for 60 min. Following 3 washings in TBS, the sections were rinsed once in distilled water (DW), and coverslipped with a non-fluorescent mounting medium. All sections were examined using a confocal laser scanning microscope (LSM510, Carl Zeiss, Oberkochen, Germany) (green: excitation wavelength 488 nm/emission filter 505 to 550 nm, red: excitation wavelength 488 nm/ emission filter over 650 nm) or a fluorescence microscope (DMI3000B, Leica microsystems, Wetzlar, Germany) (green: excitation filter 470 ± 40 nm/emission filter 525 ± 50 nm, red: excitation filter 546 ± 12 nm/emission filter 605 ± 75 nm). Emission wavelength of curcumin in water is about 550 nm when excited with wavelength 430 nm [15]. In the present study, we used merged pictures of red and green fluorescences to obtain higher-contrasted pictures (Fig. 1). Furthermore, some sections were stained with curcumin after a 5-min pretreatment with 99% formic acid (Wako).

Image processing: Aβ40- or Aβ42-positive areas (pixels) were measured in randomly selected regions of the cerebral cortex of each section using the Image J image analysis software (NIH, Bethesda, MD, U.S.A.). The means of the data were analyzed by Student's *t*-test.

RESULTS

Immunohistochemistry: Aβ40- or Aβ42-positive SPs were found in the brains of all animals except for a woodpecker (Table 1 and Fig. 2). In the brains of an AD patient, a monkey, a bear, a camel, and a APP Tg-mouse, most SPs were distinct, whereas those of dogs and cats had an indistinct boundary. In the brains of an AD patient, dogs, and a bear, Aβ42-positive SPs were observed more than Aβ40-positive SPs. In the brains of cats and a camel, the majority of SPs were positive for Aβ42 and negative for Aβ40. In a monkey and a APP Tg-mouse, there was no difference between Aβ42- and Aβ40-positive areas (Fig. 2).

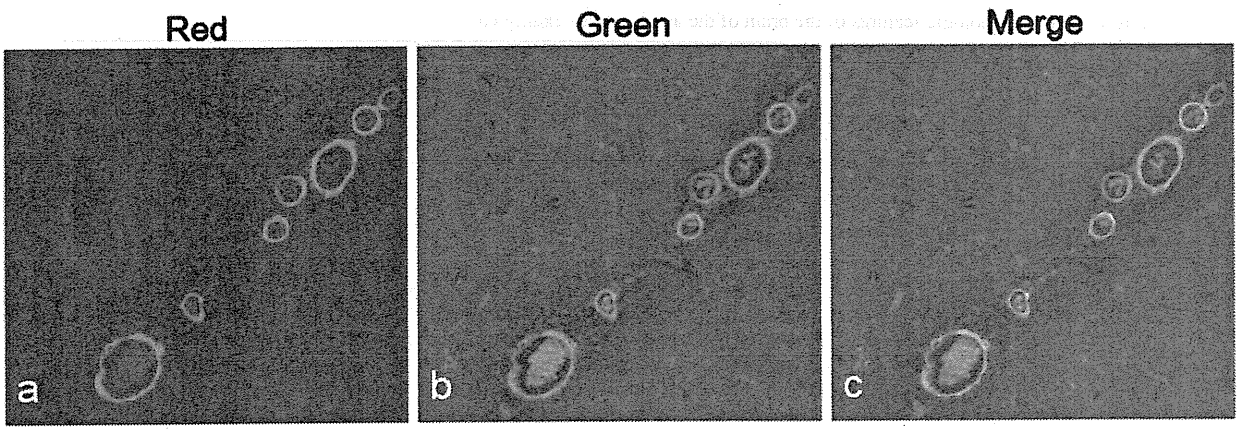

Fig. 1. A curcumin stained section of a Japanese macaque. Aβ-positive meningeal vessels are depicted with (a) red fluorescence (excitation filter 546 ± 12 nm/emission filter 605 ± 75 nm) or (b) green fluorescence (excitation filter 470±40 nm/ emission filter 525 ± 50 nm) and the pictures are merged (c).

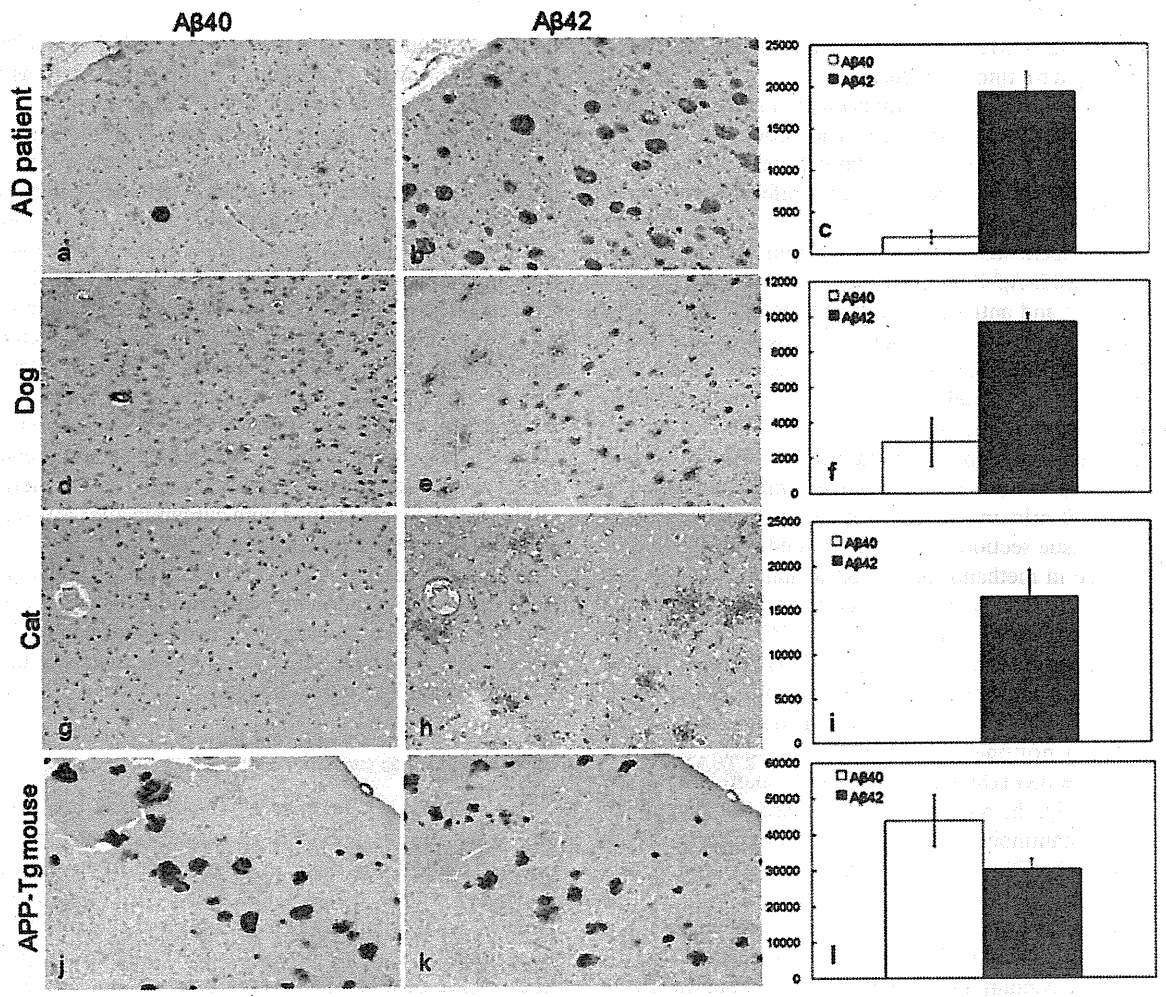

Fig. 2. Immunostain for SPs using antibodies for Aβ40 (a, d, g, j) and Aβ42 (b, e, h, k), and the semi-quantitative data (c, f, i, l) for Aβ40 (□) or Aβ42 (■). AD patient (a, b, c), dog No.9 (d, e, f), cat (g, h, i) and APP Tg-mouse (j, k, l).

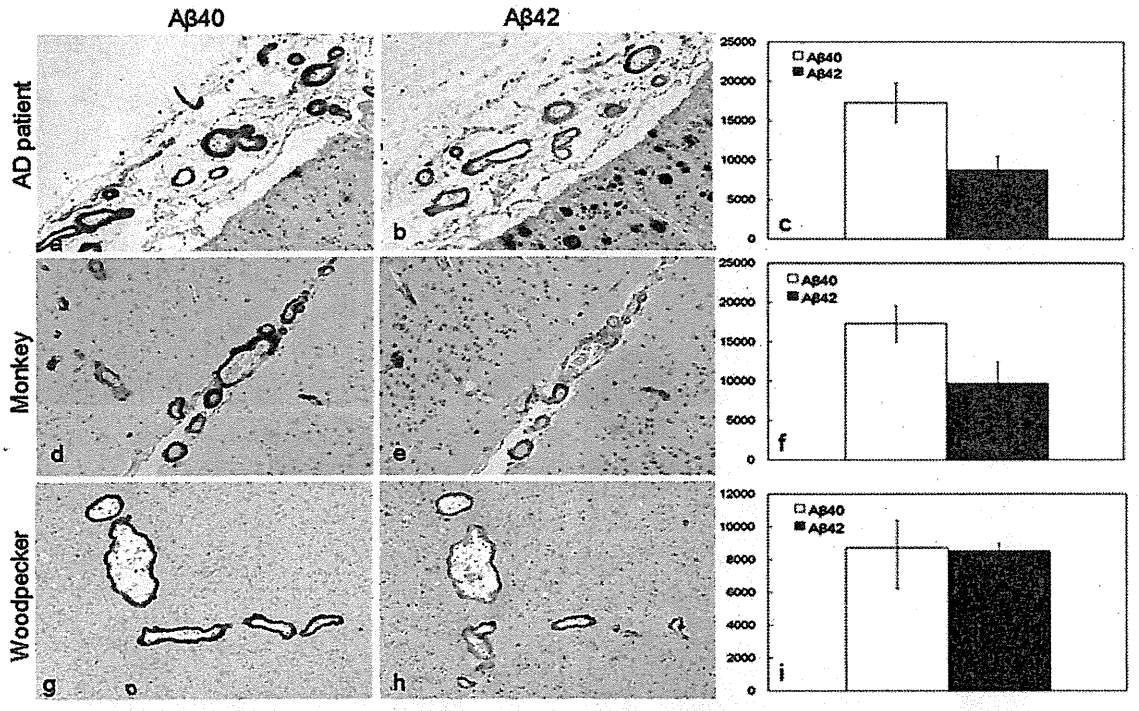

Fig. 3. Immunostain for CAA using antibodies for Aβ40 (a, d, g) and Aβ42 (b, e, h), and the semi-quantitative data (c, f, i) for Aβ40 (□) or Aβ42 (■). AD patient (a, b, c), Japanese macaque (d, e, f) and great spotted woodpecker (g, h, i).

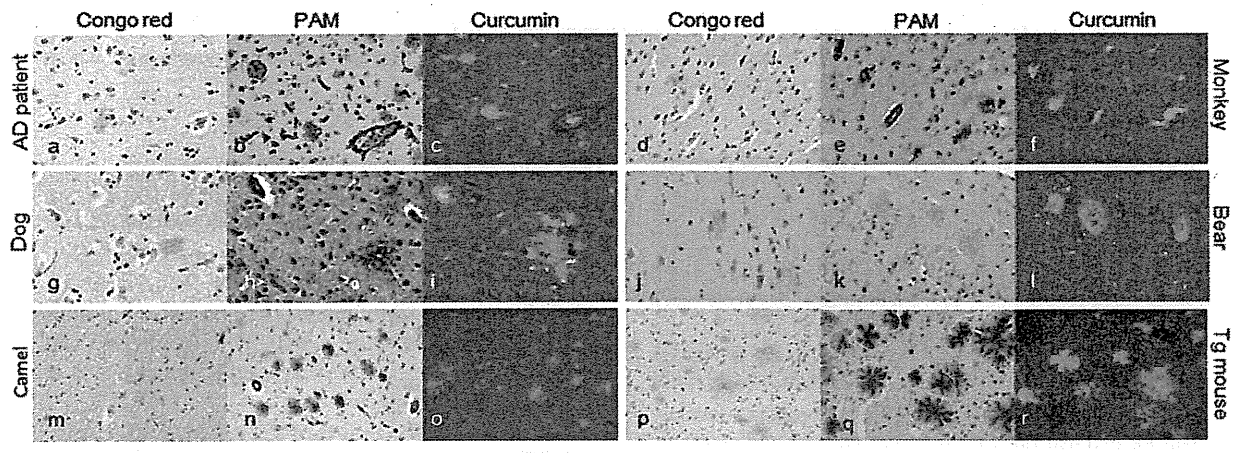

Fig. 4. Comparison of Congo red stain (a, d, g, j, m, p), PAM stain (b, e, h, k, n, q) and curcumin stain (c, f, i, l, o, r) for SPs. AD patient (a, b, c), Japanese macaque (d, e, f), dog No. 5 (g, h, i), American black bear (j, k, l), Bactrian camel (m, n, o) and APP Tg-mouse (p, q, r).

CAA was observed in the meningeal and parenchymal vessels and capillaries of all animal species excluding a camel by both Aβ42 and Aβ40 immunostains (Table 1 and Fig. 3). CAA was labeled more intensely for Aβ40 compared with that for Aβ42 (Fig. 3).

NFTs were found only in the AD brain by PHF-tau immunostain (Table 1).

Curcumin stain: SPs (Fig. 4): Both congophilic MPs and Congo red-negative DPs were observed in the AD, monkey, bear, and APP Tg-mouse brains. Curcumin stained all these SPs. DPs were found in all dogs examined, whereas a few MPs were found only in three dogs (Nos. 5, 6, and 7). Such canine MPs were intensely stained with curcumin, but canine DPs were negative. In the camel, only DPs were found and they were positive for curcumin. Aβ42-positive deposits were found in the cat brain, but they were negative for curcumin as well as Congo red and PAM.

CAA (Fig. 5): In all animals except for a camel, CAA was intensely stained with curcumin. In a woodpecker and some dogs, perivascular Aβ deposits were also intensely positive

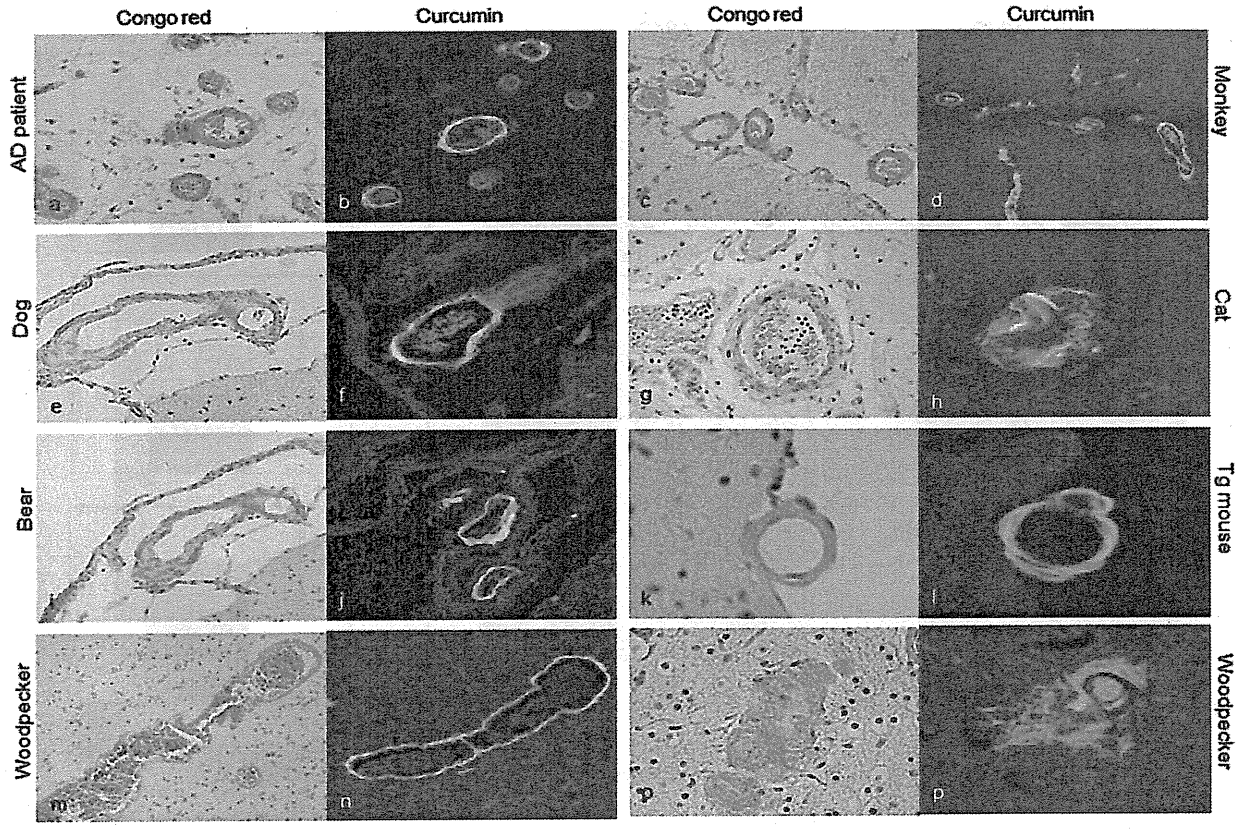

Fig. 5. Comparison of Congo red stain (a, c, e, g, i, k, m, o) and curcumin stain (b, d, f, h, j, l, n, p) for CAA. AD patient (a,b), Japanese macaque (c, d), dog No. 5 (e, f), cat (g, h), American black bear(i, j), APP Tg-mouse (k, l), great spotted woodpecker(m, n), and perivascular Aβ-positive deposits in the great spotted woodpecker (o, p).

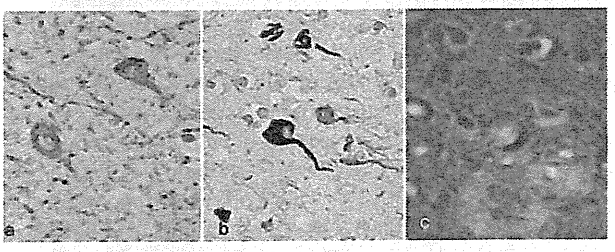

Fig. 6. NFTs in the cerebral cortex of an AD patient. Immunostain for PHF-tau (a), Gallyas silver stain (b) and curcumin stain (c).

for Congo red and curcumin (Fig. 5-o, p).

NFTs (Fig. 6): NFTs found in the AD brain were positive for Gallyas silver and curcumin. Gallyas silver stain was more sensitive than curcumin stain.

Formic acid pretreatment (Fig. 7): By formic acid pretreatment, curcumin-positive SPs and CAA in all animal species became negative.

DISCUSSION

DPs are thought to be the initial stage of plaque formation, and they are negative for Congo red [29]. In contrast, MPs are plaques of the more progressive stages, and they are positive for Congo red [28]. Both DPs and MPs can be detected by PAM stain and Aβ immunostain [25, 29]. The present study revealed that DPs were found in all animals other than the woodpecker, and MPs were found in the AD patient, monkey, dog, bear, and APP Tg-mouse (Table 1), indicating the difference of Aβ aggregation status among stages and animal species.

The shape of SPs in the APP Tg-mouse was flower-like and different from that in other animals. Artificially overexpressed APP may induce such abnormal Aβ aggregates in the mouse. In addition, SPs in the APP Tg-mouse were more strongly stained with curcumin than those in AD patients and other animal species. These results indicate that highly aggregated Aβ is apt to bind to curcumin. On the other hand, curcumin did not stain canine and feline DPs. Generally, most canine and all feline SPs are DPs [26], and they had indistinct boundaries. Feline SPs are formed in very old animals, suggesting that such feline Aβ aggregates occur at the very early stage of SP formation [18]. Thus, Aβ in canine and feline DPs may be less aggregated than that in AD patient and monkey. These findings also indicate that curcumin may bind to Aβ aggregates at later stages. Further-

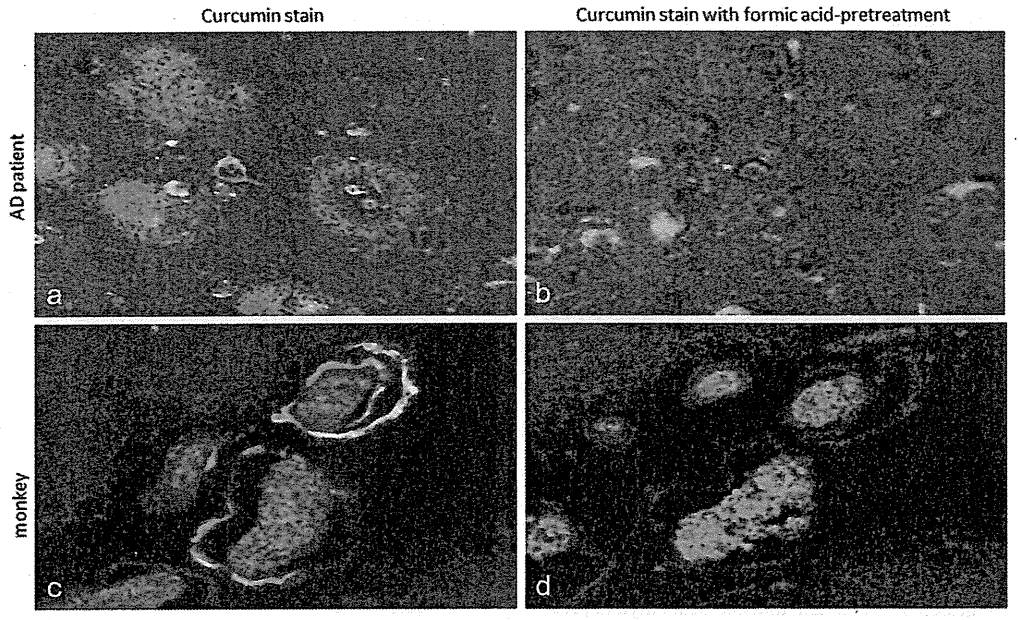

Fig. 7. Curcumin stain without formic acid pretreatment (a, c) and Curcumin stain with formic acid pretreatment (b, d). SPs of an AD patient (a, b) and CAA of a Japanese macaque (c, d).

more, DPs in the AD patient, monkey, bear, camel and APP Tg-mouse were stained with curcumin. It is thought that curcumin binds to SPs more sensitively than Congo red, since Congo red-negative DPs were positive for curcumin.

By formic acid pretreatment, the binding of curcumin to SPs, CAA, and NFTs was lost. For the Aβ immunostain, formic acid pretreatment is used to restore and reinforce Aβ immunoreactivity [12]. Formic acid more likely solubilizes Aβ-derived amyloid fibrils and therefore disrupts the polymer fibrillar configuration while exposing the Aβ epitopes. The disrupted structures enhance the immunoreactivity of the antibody to Aβ. However, Aβ could bind to neither Congo red nor curcumin when its protein structure was lost. Since the chemical structure of curcumin is partly similar to that of Congo red [30], curcumin may bind to the Aβ aggregates by the recognition of their structure by a similar manner to that of Congo red.

Generally, it is thought that SPs in human mainly consist of Aβ42, and CAA consists of Aβ40. It has also been shown that DPs of AD patients and dogs mainly consist of Aβ42, and their MPs mainly consist of Aβ40 [16]. The present study indicated that most SPs consist of Aβ42 in AD, dog, bear, camel, and cat brains, whereas most SPs consist of both Aβ42 and Aβ40 in monkey and APP Tg-mouse brains. Regarding CAA, it mainly consists of Aβ40 and Aβ42 in the AD, monkey, cat, APP Tg-mouse, and woodpecker brains, whereas CAA consists of Aβ40 in the dog and bear. Curcumin stained both SPs and CAA, which were positive for Aβ40 and/or Aβ42 in the present study. These results suggest that the binding of curcumin to Aβ does not depend on the C-terminal structure of Aβ.

In the present study, NFTs in the AD brain were stained with curcumin as described in a previous report [14]. However, the Gallyas silver stains labeled NFTs more sensitively than curcumin stain. This result indicates that curcumin binds to abnormal tau protein, but the binding activity is weaker than that to Aβ, and reveals the limited utility of curcumin stain for the detection of NFTs.

In conclusion, curcumin can bind specifically to abnormal tau proteins as well as to highly aggregated Aβ. Such curcumin binding is more sensitively than Congo red. Furthermore, curcumin stain is more simple and less nonspecific than Congo red stain. The present results clearly indicate the utility of curcumin as a specific marker for Aβ detection in various animals.

ACKNOWLEDGMENTS. This work was supported by the URAKAMI FOUNDATION. The authors would like to express their sincere gratitude to the foundation, and also to Dr. Takane Matsui, a professor of Obihiro University of Agriculture and Veterinary Medicine for his offer of valuable materials.

REFERENCES

1. Aggarwal, B. B., Kumar, A. and Bharti, A. C. 2003. Anticancer potential of curcumin: preclinical and clinical studies. *Anticancer Res.* **23**: 363–398.
2. Begum, A. N., Jones, M. R., Lim, G. P., Morihara, T., Kim, P., Heath, D. D., Rock, C. L., Pruitt, M. A., Yang, F., Hudspeth, B., Hu, S., Faull, K. F., Teter, B., Cole, G. M. and Frautschy, S. A. 2008. Curcumin structure-function, bioavailability, and efficacy in models of neuroinflammation and Alzheimer's disease. *J. Pharmacol. Exp. Ther.* **326**: 196–208.
3. Borrás, D., Ferrer, I. and Pumarola, M. 1999. Age-related

changes in the brain of the dog. *Vet. Pathol.* **36**: 202–211.
4. Braak, H., Braak, E., Ohm, T. and Bohl, J. 1988. Silver impregnation of Alzheimer's neurofibrillary changes counterstained for basophilic material and lipofuscin pigment. *Stain Technol.* **63**: 197–200.
5. Braak, H., Braak, E. and Strothjohann, M. 1994. Abnormally phosphorylated tau protein related to the formation of neurofibrillary tangles and neuropil threads in the cerebral cortex of sheep and goat. *Neurosci. Lett.* **171**: 1–4.
6. Cork, L. C., Powers, R. E., Selkoe, D. J., Davies, P., Geyer, J. J. and Price, D. L. 1988. Neurofibrillary tangles and senile plaques in aged bears. *J. Neuropathol. Exp. Neurol.* **47**: 629–641.
7. Elfenbein, H. A., Rosen, R. F., Stephens, S. L., Switzer, R. C., Smith, Y., Pare, J., Mehta, P. D., Warzok, R. and Walker, L. C. 2007. Cerebral beta-amyloid angiopathy in aged squirrel monkeys. *Histol. Histopathol.* **22**: 155–167.
8. Frautschy, S. A., Hu, W., Kim, P., Miller, S. A., Chu, T., Harris-White, M. E. and Cole, G. M. 2001. Phenolic anti-inflammatory antioxidant reversal of Abeta-induced cognitive deficits and neuropathology. *Neurobiol. Aging* **22**: 993–1005.
9. Fukuoka, A., Nakayama, H. and Doi, K. 2004. Immunohistochemical detection of beta-amyloid and beta-amyloid precursor protein in the canine brain and non-neuronal epithelial tissues. *Amyloid* **11**: 173–178.
10. Garcia-Alloza, M., Borrelli, L. A., Rozkalne, A., Hyman, B. T. and Bacskai, B. J. 2007. Curcumin labels amyloid pathology in vivo, disrupts existing plaques, and partially restores distorted neurites in an Alzheimer mouse model. *J. Neurochem.* **102**: 1095–1104.
11. Hamaguchi, T., Ono, K., Murase, A. and Yamada, M. 2009. Phenolic compounds prevent Alzheimer's pathology through different effects on the amyloid-beta aggregation pathway. *Am. J. Pathol.* **175**: 2557–2565.
12. Kitamoto, T., Ogomori, K., Tateishi, J. and Prusiner, S. B. 1987. Formic acid pretreatment enhances immunostaining of cerebral and systemic amyloids. *Lab. Invest.* **57**: 230–236.
13. Lim, G. P., Chu, T., Yang, F., Beech, W., Frautschy, S. A. and Cole, G. M. 2001. The curry spice curcumin reduces oxidative damage and amyloid pathology in an Alzheimer transgenic mouse. *J. Neurosci.* **21**: 8370–8377.
14. Mohorko, N., Repovs, G., Popović, M., Kovacs, G. G. and Bresjanac, M. 2010. Curcumin labeling of neuronal fibrillar tau inclusions in human brain samples. *J. Neuropathol. Exp. Neurol.* **69**: 405–414.
15. Mukerjee, A., Sørensen, T. J., Ranjan, A. P., Raut, S., Gryczynski, I., Vishwanatha, J. K. and Gryczynski, Z. 2010. Spectroscopic properties of curcumin: orientation of transition moments. *J. Phys. Chem. B* **114**: 12679–12684.
16. Nakamura, S., Tamaoka, A., Sawamura, N., Kiatipattanasakul, W., Nakayama, H., Shoji, S., Yoshikawa, Y. and Doi, K. 1997. Deposition of amyloid beta protein (Aβ) subtypes [Aβ40 and Aβ42(43)] in canine senile plaques and cerebral amyloid angiopathy. *Acta Neuropathol.* **94**: 323–328.
17. Nakamura, S., Nakayama, H., Goto, N., Ono, F., Sakakibara, I. and Yoshikawa, Y. 1998. Histopathological studies of senile plaques and cerebral amyloidosis in cynomolgus monkeys. *J. Med. Primatol.* **27**: 244–252.
18. Nakamura, S., Nakayama, H., Kiatipattanasakul, W., Uetsuka, K., Uchida, K. and Goto, N. 1996. Senile plaques in very aged cats. *Acta Neuropathol.* **91**: 437–439.
19. Nakamura, S., Nakayama, H., Uetsuka, K., Sasaki, N., Uchida, K. and Goto, N. 1995. Senile plaques in an aged two-humped (Bactrian) camel (Camelus bactrianus). *Acta Neuropathol.* **90**: 415–418.
20. Nakayama, H., Katayama, K., Ikawa, A., Miyawaki, K., Shinozuka, J., Uetsuka, K., Nakamura, S., Kimura, N., Yoshikawa, Y. and Doi, K. 1999. Cerebral amyloid angiopathy in an aged great spotted woodpecker (Picoides major). *Neurobiol. Aging* **20**: 53–56.
21. Podlisny, M. B., Tolan, D. R. and Selkoe, D. J. 1991. Homology of the amyloid beta protein precursor in monkey and human supports a primate model for beta amyloidosis in Alzheimer's disease. *Am. J. Pathol.* **138**: 1423–1435.
22. Roertgen, K. E., Parisi, J. E., Clark, H. B., Barnes, D. L., O'Brien, T. D. and Johnson, K. H. 1996. A beta-associated cerebral angiopathy and senile plaques with neurofibrillary tangles and cerebral hemorrhage in an aged wolverine (Gulo gulo). *Neurobiol. Aging* **17**: 243–247.
23. Rosen, R.F., Farberg, A.S., Gearing, M., Dooyema, J., Long, P. M., Anderson, D. C., Davis-Turak, J., Coppola, G., Geschwind, D. H., Paré, J. F., Duong, T. Q., Hopkins, W. D., Preuss, T. M. and Walker, L. C. 2008. Tauopathy with paired helical filaments in an aged chimpanzee. *J. Comp. Neurol.* **509**: 259–270.
24. Selkoe, D. J., Bell, D. S., Podlisny, M. B., Price, D. L. and Cork, L. C. 1987. Conservation of brain amyloid proteins in aged mammals and humans with Alzheimer's disease. *Science* **235**: 873–877.
25. Tagliavini, F., Giaccone, G., Frangione, B. and Bugiani, O. 1988. Preamyloid deposits in the cerebral cortex of patients with Alzheimer's disease and nondemented individuals. *Neurosci. Lett.* **93**: 191–196.
26. Uchida, K., Nakayama, H. and Goto, N. 1991. Pathological studies on cerebral amyloid angiopathy, senile plaques and amyloid deposition in visceral organs in aged dogs. *J. Vet. Med. Sci.* **53**: 1037–1042.
27. Uchida, K., Yoshino, T., Yamaguchi, R., Tateyama, S., Kimoto, Y., Nakayama, H. and Goto, N. 1995. Senile plaques and other senile changes in the brain of an aged American black bear. *Vet. Pathol.* **32**: 412–414.
28. Wisniewski, H. M. and Terry, R. D. 1973. Reexamination of the pathogenesis of the senile plaques. *Prog. Neuropathol.* **2**: 1–26.
29. Yamaguchi, H., Hirai, S., Morimatsu, M., Shoji, M. and Harigaya, Y. 1988. Diffuse type of senile plaques in the brains of Alzheimer-type dementia. *Acta Neuropathol.* **77**: 113–119.
30. Yang, F., Lim, G. P., Begum, A. N., Ubeda, O. J., Simmons, M. R., Ambegaokar, S. S., Chen, P. P., Kayed, R., Glabe, C. G., Frautschy, S. A. and Cole, G. M. 2005. Curcumin inhibits formation of amyloid beta oligomers and fibrils, binds plaques, and reduces amyloid *in vivo*. *J. Biol. Chem.* **280**: 5892–5901.

Journal of Alzheimer's Disease 27 (2011) 271–280
DOI 10.3233/JAD-2011-110455
IOS Press

Vitamin A has Anti-Oligomerization Effects on Amyloid-β *In Vitro*

Junichi Takasaki[a,1], Kenjiro Ono[a,1], Yuji Yoshiike[b], Mie Hirohata[a], Tokuhei Ikeda[a], Akiyoshi Morinaga[a], Akihiko Takashima[b] and Masahito Yamada[a,*]
[a]*Department of Neurology and Neurobiology of Aging, Kanazawa University Graduate School of Medical Science, Kanazawa, Japan*
[b]*Laboratory for Alzheimer's Disease, Brain Science Institute, Riken, Wako, Saitama, Japan*

Accepted 12 June 2011

Abstract. Inhibition of amyloid-β (Aβ) aggregation is an attractive therapeutic strategy for treatment of Alzheimer's disease (AD). We previously reported that vitamin A and β-carotene inhibit fibrillation of $A\beta_{40}$ and $A\beta_{42}$ (Ono et al, 2004, *Exp Neurol*). In this study, we firstly examined the effects of vitamin A (retinoic acid, retinol, and retinal), β-carotene, vitamin B2, vitamin B6, vitamin C, vitamin E, coenzyme Q10, and α-lipoic acid on oligomerization of $A\beta_{40}$ and $A\beta_{42}$ *in vitro*; vitamin A and β-carotene dose-dependently inhibited oligomerization of $A\beta_{40}$ and $A\beta_{42}$. Furthermore, retinoic acid decreased cellular toxicity by inhibition of $A\beta_{42}$ oligomerization. Second, we analyzed how vitamin A inhibits Aβ aggregation by using fluorescence spectroscopy and thioflavin T assay with two Aβ fragments, $A\beta_{1\text{-}16}$ and $A\beta_{25\text{-}35}$. A fluorescence peak of retinoic acid was greatly restrained in the presence of $A\beta_{25\text{-}35}$, and retinoic acid inhibited aggregation of $A\beta_{25\text{-}35}$, but not of $A\beta_{1\text{-}16}$, which suggest the specific binding of retinoic acid to the C-terminal portion of Aβ. Thus, vitamin A and β-carotene might be key molecules for prevention of AD.

Keywords: Alzheimer's disease, amyloid-β, oligomer, vitamin A

Supplementary data available online: http://www.j-alz.com/issues/27/vol27-2.html#supplementarydata02

INTRODUCTION

Alzheimer's disease (AD) is characterized by neuropathological features comprising amyloid deposits, neurofibrillary tangles, and neuronal loss [1, 2]. Aggregation of amyloid-β (Aβ) has been considered a critical step in AD pathogenesis. The most potent neurotoxic assemblies appear to be oligomeric rather than fibrillar in nature [3, 4].

Photo-induced cross-linking of unmodified proteins (PICUP) [5] is a useful method for characterizing oligomer size distributions and quantitative study of metastable, quaternary protein structures [6–9]. PICUP-stabilized oligomers have significant biochemical properties such as increased neurotoxic activity and β-sheet ratios of secondary structures with higher oligomer order [10–12].

We previously reported that various vitamins and their analogs, such as vitamin A [13], β-carotene [13], coenzyme Q10 (CoQ10) [14], and α-lipoic acid (LA) [15], inhibit fibrillation of $A\beta_{40}$ and $A\beta_{42}$ *in vitro*.

Using PICUP, electron microscopy (EM), atomic force microscopy (AFM), and cytotoxicity assay, we examined the effects of vitamins and their analogs on oligomerization of $A\beta_{40}$ and $A\beta_{42}$ *in vitro*. Further, we investigated the binding site of vitamin A using fluorescence spectroscopy and thioflavin T (ThT) assay with Aβ fragments.

[1]These authors contributed equally to this work.

*Correspondence to: Masahito Yamada, MD, PhD, 13-1 Takara-machi, Kanazawa 920-8640, Japan. Tel.: +81 76 265 2290; Fax: +81 76 234 4253; E-mail: m-yamada@med.kanazawa-u.ac.jp.

MATERIALS AND METHODS

Peptide, chemicals, and reagents

$A\beta_{40}$, $A\beta_{42}$, $A\beta_{1\text{-}16}$, and $A\beta_{25\text{-}35}$ were obtained from Peptide Institute Inc. (Osaka, Japan). Glutathione *S*-transferase (GST) was obtained from Sigma-Aldrich Co. (St. Louis, MO). Chemicals were obtained from Sigma-Aldrich Co. and were of the highest purity available. Water was produced using Milli-Q system (Millipore Corp., Bedford, MA).

PICUP

PICUP was performed as described previously [10, 11]. Briefly, the general method was to mix 25 μM $A\beta_{40}$, $A\beta_{42}$ or 250 μM GST (Sigma-Aldrich, St. Louis, MO) with 4 mM tris(2,2′-bipyridyl) dichlororuthenium(II) hexahydrate (Ru(bpy)) and 80 mM ammonium persulfate (APS) in 10 mM phosphate (pH 7.4). Test compounds (retinoic acid, retinol, retinal, βcarotene, vitamin B2, vitamin B6, vitamin C, vitamin E, CoQ10, and LA) (Sigma-Aldrich) were diluted with 10 mM phosphate (pH 7.4) to produce concentrations of 25 and 250 μM. The mixtures were then irradiated for 1 s with visible light, and the reaction was quenched with 1 M dithiothreitol (Invitrogen, Carlsbad, CA) in water. Each sample was electrophoresed on a 10–20% Tris-tricine gradient gel (Invitrogen) and visualized by silver staining (SilverXpress, Invitrogen). Densitometry was then performed using a luminescent image analyzer (LAS 4000 mini, Fujifilm, Tokyo) and image analysis software (Multi gauge version 3.2, Fujifilm). The intensity of each band in a lane from the SDS gel was normalized to the sum of the intensities of all the bands in that lane, according to the formula $R_i = I_i / \sum_{i=1}^{n} I_i$, where R_i is the normalized intensity of band i and I_i is the intensity of each band i. R_i varies from 0–1.

EM

EM was perfomed as described previously [10, 11]. Samples were examined using a JEOL JEM-1210 transmission electron microscope. 10 μl of same sample with that used in PICUP experiments were spotted onto glow-discharged, carbon-coated Formvar grids (Okenshoji, Tokyo, Japan) and incubated for 20 min. The droplet was then displaced with an equal volume of 2.5% (v/v) glutaraldehyde solution and incubated for an additional 5 min. Finally, the peptide was stained with 8 μl of 1% (v/v) filtered (0.2 μm) uranyl acetate solution (Electron Microscopy Sciences). This solution was wicked off, and the grid air-dried.

AFM

AFM was performed as described previously [10, 11]. For AFM, peptide solutions were characterized using a Nanoscope IIIa scanning probe microscope (Veeco Digital Instruments, Santa Barbara, CA). All measurements were carried out in the tapping mode under ambient conditions using single-beam silicon cantilever probes. A 10 μl aliquot was spotted onto freshly cleaved mica (Veeco Digital Instruments), incubated at room temperature for 5 min, rinsed with water, and then blown dry with air.

Effective concentration (EC_{50})

EC_{50} was defined as concentrations of compounds required to inhibit $A\beta_{40}$ or $A\beta_{42}$ oligomerization to 50% of the control value. EC_{50} was calculated using the GraphPad Prism software (version 4.0a).

Preparation of cytotoxicity experiments

For the preparation of cytotoxicity experiments, PICUP reagents and retinoic acid were removed from Aβ samples (25 μM un-cross-linked $A\beta_{42}$, 25 μM cross-linked $A\beta_{42}$, or 25 μM cross-linked $A\beta_{42}$ with 250 μM retinoic acid) by size exclusion chromatography (SEC) as described previously [11]. 1.5 cm diameter cylindrical columns were packed manually with 2 g of Bio-Gel P2 Fine (Bio-Rad Laboratories, Hercules, CA), which produced a 6 ml column volume. The column first was washed twice with 25 ml of 50 mM NH_4HCO_3, pH 8.5. Two-hundred sixteen μl of cross-linked sample then was loaded. The column was eluted with the same buffer at a flow rate of ≈0.15 ml/min. The first 1 ml of eluate was collected. The fractionation range of the Bio-Gel P2 column is 100–1800 Da. $A\beta_{42}$ peptide thus elutes in the void volume whereas Ru(bpy) (MW = 748.6), APS (MW = 228.2), retinoic acid (MW = 300.4), and DTT (MW = 154.2) enter the column matrix and are separated from Aβ. Fractions were lyophilized immediately after collection. Reconstitution of the lyophilizates to a concentration of 25 μM in 10 mM sodium phosphate, pH 7.4, followed by the SDS-PAGE analysis, showed that removal of reagents and retinoic acid, lyophilization, and reconstitution did not alter the oligomer composition of any of the peptide populations under study (Supplementary Fig. 1; available

online: http://www.j-alz.com/issues/27/vol27-2.html #supplementarydata02). Finally, Aβ samples were prepared at 0.2, 2, and 20 μM in 10 mM sodium phosphate, pH 7.4.

Cell culture

Human embryonic kidney (HEK) 293 cells were cultured in 75-cm^2 flasks (Corning, Corning, NY) in Dulbecco's modified Eagle's medium (DMEM) (Sigma-Aldrich) containing 10% fetal bovine serum and incubated in a humidified chamber (85% humidity) containing 5% CO_2 at 37°C. One day before Aβ sample treatment, the cell culture medium was replaced with serum-free DMEM, and the cells were trypsinized and re-plated onto precoated 96-well plates with poly-D-lysine at a final cell density of 20,000 cells/well.

Cytotoxicity assays

We tested the toxicity of un-cross-linked, cross-linked, and cross-linked with retinoic acid of $A\beta_{42}$ after removal of the reagents and reconstitution using 3-[4,5-dimethylthiazol-2-yl]-2,5-diphenyltetrazolium bromide (MTT) assay. MTT assays are a rapid and sensitive method for determination of gross Aβ toxicity in cultures of dissociated cells [16]. Aliquots of 50 μl were added to HEK cells to yield final Aβ concentrations of 0.1, 1, and 10 μM. Twenty-two hours after the cells were incubated with peptide samples, MTT was added to each well, and the plates were kept in a CO_2 incubator for an additional 2 h. The cells were then lysed by adding lysis solution (50% dimethylformamide, 20% SDS at pH 4.7) and were incubated overnight. The degree of MTT reduction (i.e., cell viability) in each sample was subsequently assessed by measuring absorption at 590 nm at room temperature using a plate reader (PerkinElmer, Turku, Finland). Background absorbance values, as assessed from cell-free wells, were subtracted from the absorption values of each test sample. Controls included medium with 10 mM sodium phosphate. We confirmed that 50% (vol/vol) 10 mM sodium phosphate did not influence the absorbance of the medium only. The absorbance measured from twelve wells were averaged, and reported as mean ± S.E. percentage of cell viability $V = 100 - ((A_{\text{medium}} - A_{A\beta})/(A_{\text{medium}})) \times 100$, where $A_{A\beta}$ and A_{medium} were absorbance values from Aβ-containing samples and medium with 10 mM sodium phosphate, respectively.

Fluorescence spectroscopy characterizing fluorescence of retinoic acid

Fluorescence emission of retinoic acid in the presence or absence of Aβ fragment [$A\beta_{1\text{-}16}$ or $A\beta_{25\text{-}35}$] was characterized as described previously [17] on a Hitachi F-7000 fluorescence spectrophotometer (Tokyo, Japan). The reaction mixtures (200 μL) containing 25 μM retinoic acid, 0–2.5 μM $A\beta_{1\text{-}16}$ or $A\beta_{25\text{-}35}$, and 10 mM phosphate buffer, pH 7.4 were analyzed at 25°C with a black microfluorimeter cell (GL Sciences Inc., Tokyo, Japan). Excitation and emission fluorescence spectra were obtained immediately after the reaction mixture was made. Excitation and emission were scanned in the range of 200–600 nm and 200–600 nm, respectively. The scanning speed was 2400 nm/min, and excitation and emission slits were set at 5 and 5 nm, respectively. Every scanning was finished in 5 min, and the peak fluorescence intensities (excitation at 485 nm and emission at 600 nm for retinoic acid) were recorded.

Peptide aggregation

Aggregation assay was performed as described elsewhere [13]. The reaction mixture contained 25 μM $A\beta_{1\text{-}16}$ or $A\beta_{25\text{-}35}$, 0, 25 or 250 μM retinoic acid, and 10 mM phosphate (pH 7.4). 0.6 ml aliquot of Aβ solution prepared above was placed in a 1 ml microcentrifuge tube. The tubes were incubated at 37°C for 0–48 h without agitation.

ThT assay

A fluorescence spectroscopic study was performed as described before [13] on a Hitachi F-2500 fluorescence spectrophotometer (Tokyo, Japan). Optimum fluorescence measurements were obtained at the excitation and emission wavelengths of 445 and 490 nm, with the reaction mixture containing 5 μM ThT (Wako Pure Chemical Industries Ltd, Osaka, Japan) and 50 mm of glycine-NaOH buffer, pH 8.5.

Statistical analysis

One-way factorial ANOVA followed by Bonferroni *post hoc* comparisons were used to determine statistical significance among data sets. These tests were implemented within GraphPad Prism software (version 4.0a, GraphPad Software, Inc., San Diego, CA). Significance was defined as $p < 0.05$.

RESULTS

Effects of vitamins and their analogs on Aβ oligomerization

In the absence of cross-linking, only $A\beta_{40}$ monomers (Fig. 1A, lane 2) or $A\beta_{42}$ monomers and trimers (Fig. 1B, lane 2) were observed. The $A\beta_{42}$ trimer band has been shown to be an SDS-induced artifact [18].

25 μM $A\beta_{40}$ cross-linked without vitamins existed as a mixture of monomers and oligomers of orders 2–4 (Fig. 1A, lane 3), whereas that cross-linked with 25 μM retinoic acid, retinol, retinal, or β-carotene ($A\beta_{40}$:compound ratio = 1 : 1) existed as monomers, dimers, trimers, and weak tetramers (Fig. 1A, lanes 6, 8, 10, and 12). $A\beta_{40}$ cross-linked with 250 μM retinoic acid ($A\beta_{40}$: compound ratio = 1 : 10) existed as monomers and weak dimers (Fig. 1A, lane 7). Similar patterns were observed for $A\beta_{40}$ cross-linked with 250 μM retinol or retinal (Fig. 1A, lanes 9 and 11), but $A\beta_{40}$ cross-linked with 250 μM β-carotene existed as monomers and oligomers of orders 2–3 (Fig. 1A, lane 13).

$A\beta_{42}$ cross-linked without vitamins existed as a mixture of monomers and oligomers of orders 2–6 (Fig. 1B, lane 3). $A\beta_{42}$ cross-linked with 25 μM retinoic acid ($A\beta_{42}$: compound ratio = 1 : 1) existed as monomers and oligomers of orders 2–5 (Fig. 1B, lane 6). However, $A\beta_{42}$ cross-linked with 25 μM retinol or retinal existed as monomers and oligomers of orders 2–5 and weaker hexamers (Fig. 1B, lanes 8

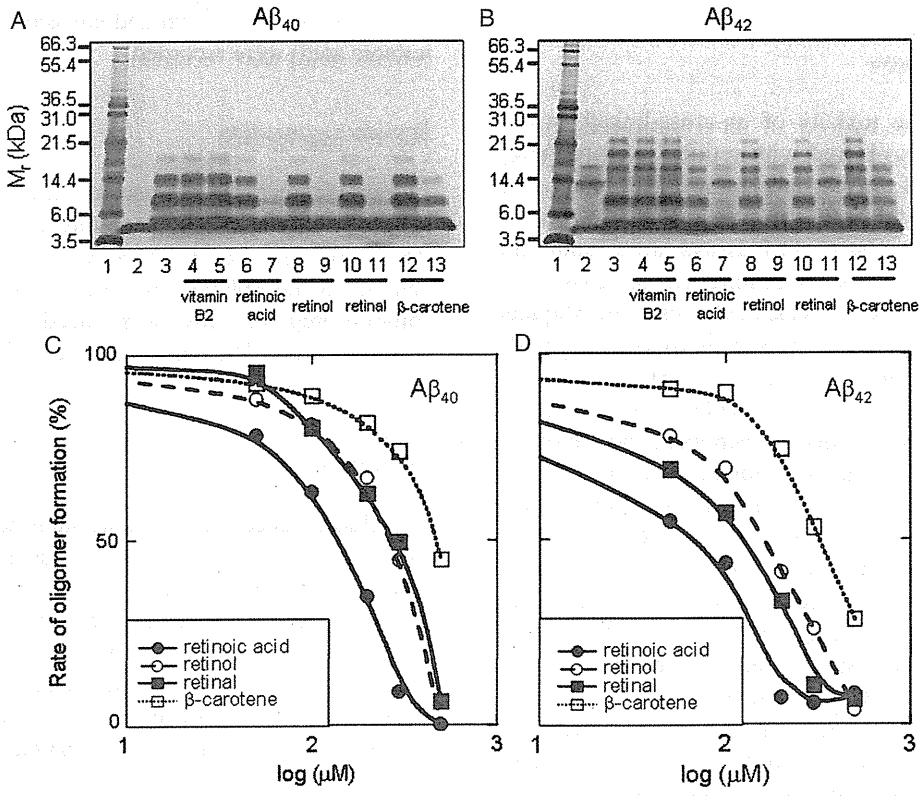

Fig. 1. Aβ oligomerization (A and B) and dose-dependent inhibition of Aβ oligomerization (C and D). PICUP, which was followed by SDS-PAGE and silver staining, was used to determine the effects of 25 and 250 μM vitamin B2, retinoic acid, retinol, retinal, or β-carotene on oligomerization of $A\beta_{40}$ (A) or $A\beta_{42}$ (B). Lane 1, molecular weight markers; lane 2, Aβ alone (un-cross-linked); lane 3, Aβ alone (cross-linked); lane 4, Aβ with vitamin B2 (25 μM); lane 5, Aβ with vitamin B2 (250 μM); lane 6, Aβ with retinoic acid (25 μM); lane 7, Aβ with retinoic acid (250 μM); lane 8, Aβ with retinol (25 μM); lane 9, Aβ with retinol (250 μM); lane 10, Aβ with retinal (25 μM); lane 11, Aβ with retinal (250 μM); lane 12, Aβ with β-carotene (25 μM); and lane 13, Aβ with β-carotene (250 μM). PICUP, which was followed by SDS-PAGE and silver staining, was used to determine the effects of 0, 25, 50, 100, 150, and 250 μM retinoic acid (filled circles), retinol (open circles), retinal (filled squares), or β-carotene (open squares) on oligomerization of $A\beta_{40}$ (C) or $A\beta_{42}$ (D). Points represent means of four independent experiments. At all points, standard errors were within symbols. The average without compounds was regarded as 100%. Each gel is representative of each of three independent experiments.

and 10), and $A\beta_{42}$ cross-linked with 25 μM β-carotene existed as monomers through pentamers and strong hexamers (Fig. 1B, lane 12). $A\beta_{42}$ cross-linked with 250 μM retinoic acid ($A\beta_{42}$: compound ratio = 1 : 10) existed as monomers and trimers (Fig. 1B, lane 7). Similarly, $A\beta_{42}$ cross-linked with 250 μM retinol or retinal produced the same bands (Fig. 1B, lanes 9 and 11), whereas $A\beta_{42}$ cross-linked with 250 μM β-carotene existed as monomers and oligomers of orders 2–4 (Fig. 1B, lane 13).

As shown in Figs. 1C, D, and Supplementary Fig. 2, oligomerization of both $A\beta_{40}$ and $A\beta_{42}$ were blocked in a dose-dependent manner by retinoic acid, retinol, retinal, and β-carotene. In the $A\beta_{40}$ system, EC_{50} of retinoic acid was 61.5 ± 2.02 (mean ± S.E., $n = 3$) μM. EC_{50} of retinol, retinal, and β-carotene was 122.3 ± 5.81, 115.6 ± 4.62, and 128.0 ± 3.39 μM, respectively. In the $A\beta_{42}$ system, EC_{50} of retinoic acid, retinol, retinal, and β-carotene was 29.4 ± 1.37, 46.6 ± 6.1, 69.5 ± 6.5, and 115.3 ± 6.43 μM, respectively. The overall activity of the four compounds examined was in the order of retinoic acid > retinol = retinal > β-carotene.

Vitamin B2 had no inhibitory effect on oligomerization (Figs. 1A and B, lanes 4 and 5). Similarly, vitamins B6, C, E, CoQ10, and LA had no inhibitory effect on oligomerization (Supplementary Fig. 3).

It was possible that the strong inhibition of Aβ oligomerization could have resulted from an effect of the inhibitor on the PICUP chemistry itself. To evaluate this possibility, cross-linking reactions were also performed on GST (~26 kDa), a positive control for the cross-linking chemistry. Un-cross-linked GST exhibited a strong monomer band and a relatively weak dimer band. Cross-linking produced a strong dimer band, expected because GST exists normally as a homodimer, as well as higher-order cross-linked species. No alterations in GST cross-linking were observed in the presence of retinoic acid, retinol, retinal, or β-carotene at either of the two compound: protein ratios tested, 1 : 1 or 10 : 1. Thus, the significant inhibition of $A\beta_{40}$ and $A\beta_{42}$ oligomerization is from a direct interaction with retinoic acid, retinol, retinal, or β-carotene.

Aβ assembly morphology

To determine the morphologies of the assemblies formed following Aβ cross-linking with or without 250 μM retinoic acid, we examined cross-linked samples by EM and AFM. Un-cross-linked $A\beta_{40}$ produced irregular, globular structures that often had thread-like components. The average diameter (d) of the globular structures was 1.43 nm (Fig. 2A; Table 1). Analysis of cross-linked oligomers revealed populations with much larger d ($d = 10.69$ nm; Table 1). The structures were more complex, including those that appeared to be composed of globular subunits attached to each other forming twisted, rope-like structures (Fig. 2B). However, the structures of $A\beta_{40}$ cross-linked with 250 μM retinoic acid were similar to those of un-cross-linked $A\beta_{40}$ (Fig. 2C), with $d = 1.51$ nm (Table 1). Similar data were obtained from EM analysis of $A\beta_{42}$. Diameters of un-cross-linked $A\beta_{42}$, cross-linked $A\beta_{42}$, and $A\beta_{42}$ cross-linked with 250 μM retinoic acid were 2.15, 21.22, and 2.18 nm, respectively (Figs. 2G–I, Table 1).

We next studied oligomer morphology by AFM. Un-cross-linked $A\beta_{40}$ had the average height (h) of 0.20 nm (Fig. 2D; Table 1). Larger structures with h of 0.88 nm were observed for $A\beta_{40}$ after cross-linking (Fig. 2E; Table 1). The structures of $A\beta_{40}$ cross-linked with 250 μM retinoic acid were smaller than those of cross-linked $A\beta_{40}$ ($h = 0.34$ nm; Fig. 2F; Table 1). The average heights of un-cross-linked $A\beta_{42}$, cross-linked $A\beta_{42}$, and $A\beta_{42}$ cross-linked with 250 μM retinoic acid were 0.31, 1.09, and 0.36 nm, respectively (Figs. 2J–L; Table 1).

Cellular toxicity

The ability of retinoic acid to inhibit formation of low-n Aβ oligomers suggested that it might be useful in blocking Aβ-mediated cellular toxicity. To address this question, we used HEK 293 cells to perform MTT assay [19] to probe cellular metabolism. When un-cross-linked and cross-linked $A\beta_{42}$ were added immediately to cells at final concentration of 1 μM, their cell viabilities were ~57% and ~47%, respectively, as well as showing that cross-linked $A\beta_{42}$ were significantly more toxic than un-cross-linked $A\beta_{42}$ ($p < 0.01$) (Fig. 3). Treatment of $A\beta_{42}$ with retinoic acid reduced the cytotoxicity to ~16%, which was a highly significant reduction relative to cross-linked $A\beta_{42}$ as well as un-cross-linked $A\beta_{42}$ ($p < 0.01$) (Fig. 3). Similar observations were made in experiments with $A\beta_{42}$ at 10 μM retinoic acid. Un-cross-linked and cross-linked $A\beta_{42}$ displayed ~56% and ~36% cell viability levels. Retinoic acid treatment increased cell viability up to 62.5% significantly ($p < 0.01$) (Fig. 3).

In experiments with $A\beta_{42}$ at 0.1 μM, un-cross-linked and cross-linked $A\beta_{42}$ displayed ~73% and

~67% cell viability levels, respectively, although cross-linked $A\beta_{42}$ (non-significantly) towards modestly higher toxicity. Retinoic acid treatment increased cell viability ~94% higher than untreated cross-linked $A\beta_{42}$ as well as un-cross-linked $A\beta_{42}$ ($p < 0.01$) (Fig. 3).

Thus, retinoic acid was highly effective inhibitors of low-n $A\beta_{42}$ oligomer-induced cellular toxicity.

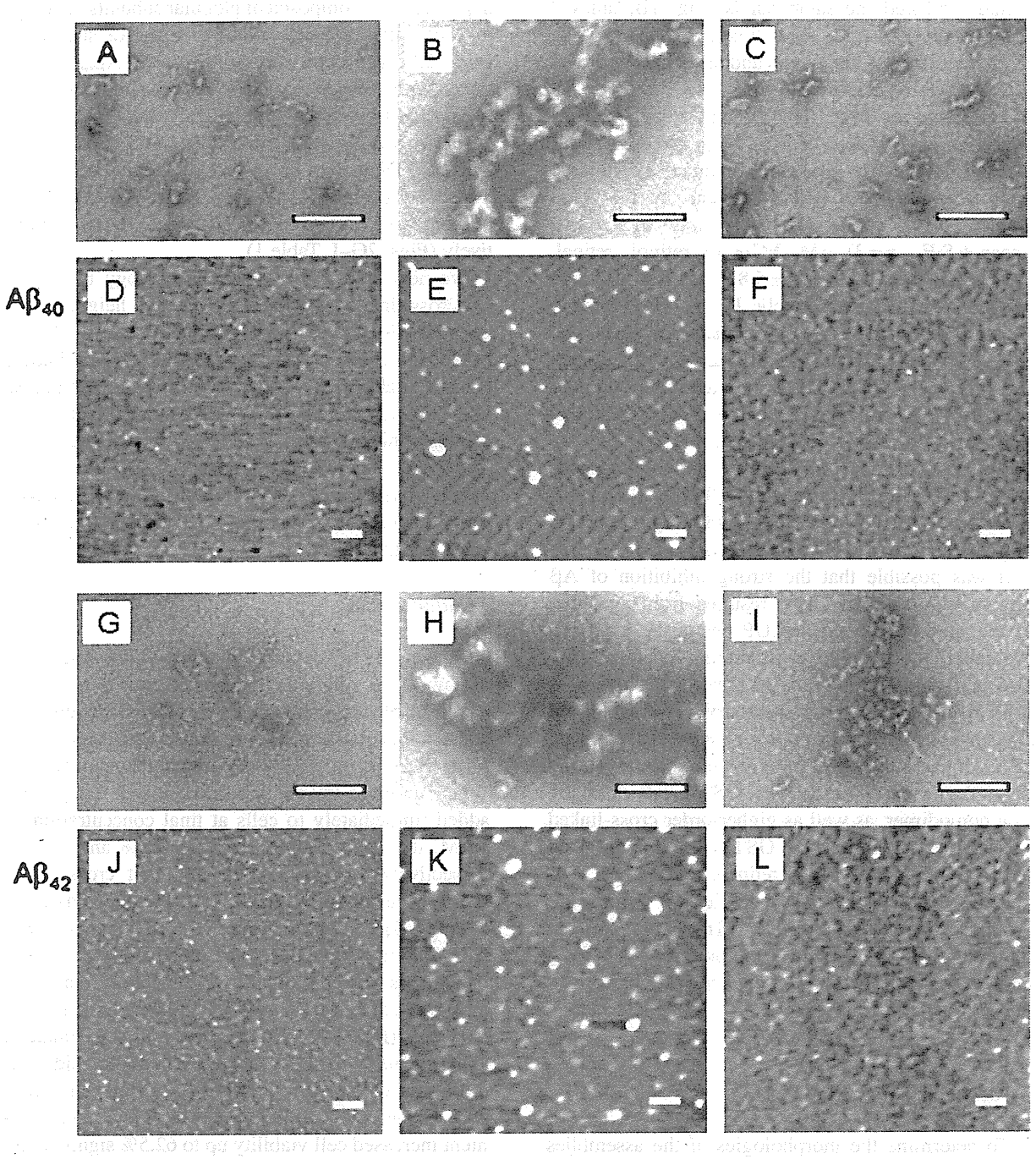

Fig. 2. Morphological analysis of $A\beta_{40}$ (A, B, and C) or $A\beta_{42}$ (G, H, and I) assemblies by EM. Un-cross-linked Aβ alone (A and G), cross-linked Aβ alone (B and H), and Aβ cross-linked with 250 μM retinoic acid (C and I) were examined by EM. Morphological analysis of $A\beta_{40}$ (D, E, and F) or $A\beta_{42}$ (J, K, and L) assemblies by AFM. Un-cross-linked Aβ alone (D and J), cross-linked Aβ alone (E and K), and Aβ cross-linked with 250 μM retinoic acid (F and L) were examined by AFM (Scale bars: 100 nm.).